Research Square

Preprints are preliminary reports that have not undergone peer review.
They should not be considered conclusive, used to inform clinical practice,
or referenced by the media as validated information.

Ecological risk from anthropogenic stressors and their key drivers exhibit scale dependence

Zhiyuan Lu
Hebei Normal University
Xueqi Liu
Hebei Normal University
Lu Wang
Hebei Normal University
Huanyang Zhao
Hebei Normal University
Hao Li
lihao@hebtu.edu.cn

Hebei Normal University

Research Article

Keywords: Ecological risk assessment, Anthropogenic stressor, Bayesian Belief Network, Geographically weighted regression, Multiscale geographically weighted regression, Scale dependence

Posted Date: February 24th, 2026

DOI: https://doi.org/10.21203/rs.3.rs-8902232/v1

License: This work is licensed under a Creative Commons Attribution 4.0 International License.
Read Full License

Additional Declarations: No competing interests reported.

Ecological risk from anthropogenic stressors and their key drivers exhibit scale dependence

Zhiyuan Lu[1, 2, 3, 4], Xueqi Liu[1, 2, 3], Lu Wang[1, 2, 3], Huanyang Zhao[1, 2, 3], Hao Li[1, 2, 3*]

1 *College of Life Sciences, Hebei Normal University, No. 20, East Road of South 2nd Ring, Yuhua District, Shijiazhuang 050024, China*
Tel: 86-311-80787550; Fax: 86-311-80787500
Email: lihao@hebtu.edu.cn (H.L.)

2 *Hebei Collaborative Innovation Center for Eco-Environment, No. 20, East Road of South 2nd Ring, Yuhua District, Shijiazhuang 050024, China*
Tel: 86-311-80787550; Fax: 86-311-80787500

3 *Hebei Key Laboratory of Animal Physiology, Biochemistry and Molecular Biology, No. 20, East Road of South 2nd Ring, Yuhua District, Shijiazhuang 050024, China*
Tel: 86-311-80787550; Fax: 86-311-80787500

4 *College of Life Sciences, Cangzhou Normal University, Cangzhou 061001, China*
Tel: 86-317-5667878; Fax: 86-311-5667878

*Corresponding author

Abstract: Robust and spatially explicit ecological risk assessments (ERAs) are essential for informing effective risk mitigation strategies. However, existing studies have insufficiently explored spatial variability in the interactions among multi-level drivers of ecological risk. Integrating Bayesian Belief Networks (BBNs) with geographically weighted regression (GWR), this study proposes a spatially explicit framework for assessing ecological risk from multiple anthropogenic stressors, and applies it to the Beijing–Tianjin–Hebei (BTH) region of North China. Results indicate that cumulative stressor risk, aggregated from agricultural production, non-cropping livelihood activities, and urbanization, exhibits pronounced spatial clustering, with urbanization acting as a key leverage point in shaping cumulative risk. These high-risk clusters delineate priority areas for conservation and targeted mitigation. These findings highlight the importance of explicitly accounting for compound stressors and incorporating finer-scale socioeconomic indicators to enhance the robustness and policy relevance of ERAs. Spatial analyses further reveal strong scale dependence in ecological risk and its drivers, while the effects of anthropogenic stressors on risk exhibit pronounced spatial heterogeneity, reflecting the combined influence of localized socioeconomic processes and broader regional linkages. Based on these insights, differentiated risk mitigation strategies tailored to dominant local stressors are proposed. Overall, this study demonstrates the value of integrating probabilistic modeling with spatially adaptive regression techniques for capturing compound stressor effects and spatial heterogeneity in ERAs, thereby enhancing the policy relevance of ERAs for sustainable land use planning and regional risk governance.

Key words: Ecological risk assessment; Anthropogenic stressor; Bayesian Belief Network; Geographically weighted regression; Multiscale geographically weighted regression; Scale dependence

1. Introduction

Ecological risk refers to the potential for adverse effects on ecosystems arising from exposure to natural and anthropogenic stressors (Bartell, 2008; Suter and Norton, 2019; Wang et al., 2024). Escalating ecological risks have contributed to accelerating biodiversity loss (CBD, 2022; Urban, 2024), widespread ecosystem degradation (Fu et al., 2023; Li et al., 2021), and growing threats to human well-being (IPBES, 2019; United Nations, 2024). These adverse outcomes collectively undermine progress toward the Sustainable Development Goals (SDGs) (IPBES, 2019). Consequently, robust and spatially ERAs are essential for informing effective risk mitigation strategies and supporting the achievement of SDGs.

ERA is a scientific process used to evaluate the likelihood and severity of adverse effects on ecosystems arising from exposure to natural and anthropogenic stressors (Suter and Norton, 2019; USEPA, 2025). In practice, ERA is frequently challenged by multi-stressor contexts (Carriger and Barron, 2020; Helle et al., 2016), pronounced spatio-temporal variability in stressor intensity and distribution (Phan et al., 2016; Sperotto et al., 2017), and incomplete understanding of underlying risk mechanisms (Ayre and Landis, 2012; Malekmohammadi and Tayebzadeh Moghadam, 2018). Together, these factors substantially increase the complexity and uncertainty of ERA.

To address the growing complexity and uncertainty in ERA, a wide range of statistical and spatial analytical tools have been applied, including multivariate regression (Dormann et al., 2018), machine learning (Meyer et al., 2019), and geographically weighted models (Fotheringham et al., 2017). These approaches have enhanced the

identification of key risk drivers and the characterization of spatial heterogeneity and nonlinear relationships in ecological risk patterns (Dormann et al., 2018; Meyer et al., 2019). However, many conventional methods remain limited in their ability to explicitly represent causal structures, integrate heterogeneous data sources, and propagate uncertainty across interacting stressors and ecosystem components (Carriger et al., 2016).

BBNs provide a probabilistic, causal modeling framework well suited to ERA under multi-stressor conditions and data limitations (Kaikkonen et al., 2021). By integrating empirical data, expert knowledge, and scenario-based inference, BBNs enable transparent representation of cumulative and compound risks while explicitly accounting for uncertainty (Landuyt et al., 2013; Uusitalo, 2007). Importantly, BBNs can be readily integrated with GIS analysis frameworks, enabling probabilistic risk inference to be mapped and interpreted in a spatially explicit context (Gonzalez-Redin et al., 2016; Landuyt et al., 2015; Liu et al., 2023). This integrative capability offers a promising pathway for advancing spatially explicit ERA.

Recent studies demonstrate the increasing use of BBNs in ERA to address complex, multi-stressor systems. Li et al. (2018) applied BBNs to assess forest landscape degradation risk in North China, highlighting the roles of land use policy and human disturbance. Extending causal risk frameworks, Du et al. (2023) integrated BBNs with a causal driver–pressure–state–response–oriented framework to support ecological security early warning and scenario simulation, enhancing decision relevance. Beyond terrestrial contexts, Martinez-Megias et al. (2023) used BBNs to assess the combined

effects of climate change and pesticide practices on ecological risks in protected wetlands. More broadly, Perez et al. (2022) emphasized the value of BBNs for environmental and ecological health risk assessment by explicitly representing causal relationships and uncertainty. Despite these advances, existing studies often focus on specific stressors or single management contexts, leaving the spatial variability in interactions among multi-level drivers of ecological risk insufficiently explored.

This study aims to develop a BBN-based ERA framework for predictive inference of regional ecological risk in spatially explicit contexts. Using the BTH region in North China as a case study, the framework predicts spatial patterns of cumulative ecological risk and individual anthropogenic stressor risks, identifies key risk drivers at stressor and plot-indicator levels, and examines spatial variability of cumulative risk and its dominant drivers across functional zones. The proposed framework enhances spatially explicit ERA and improves understanding of ecological risk mechanisms under spatial complexity and heterogeneity.

2. Materials and methods

2.1 Study area

The BTH region, comprising Beijing, Tianjin, and Hebei Province, is the largest urban agglomeration in North China, covering 216,000 km². The topography slopes from high elevations in the northwest to lowlands in the southeast (Figure 1(a)). Functionally, the region is divided into three functional zones: the northwest ecological conservation zone, the eastern agricultural production zone, and the central urban development zone (Figure 1(b)) (Chinese State Council, 2010; Ministry of Natural Resources, 2023). The

northwest ecological conservation zone is characterized by forests and grasslands in mountainous areas, whereas the eastern agricultural production zone on the North China Plain is dominated by croplands. The central urban development zone consists largely of built-up areas (Yang and Huang, 2024), accommodating 32.5% of the regional population (35.47 million), mainly concentrated in Beijing and Tianjin (Figure 1(c)).

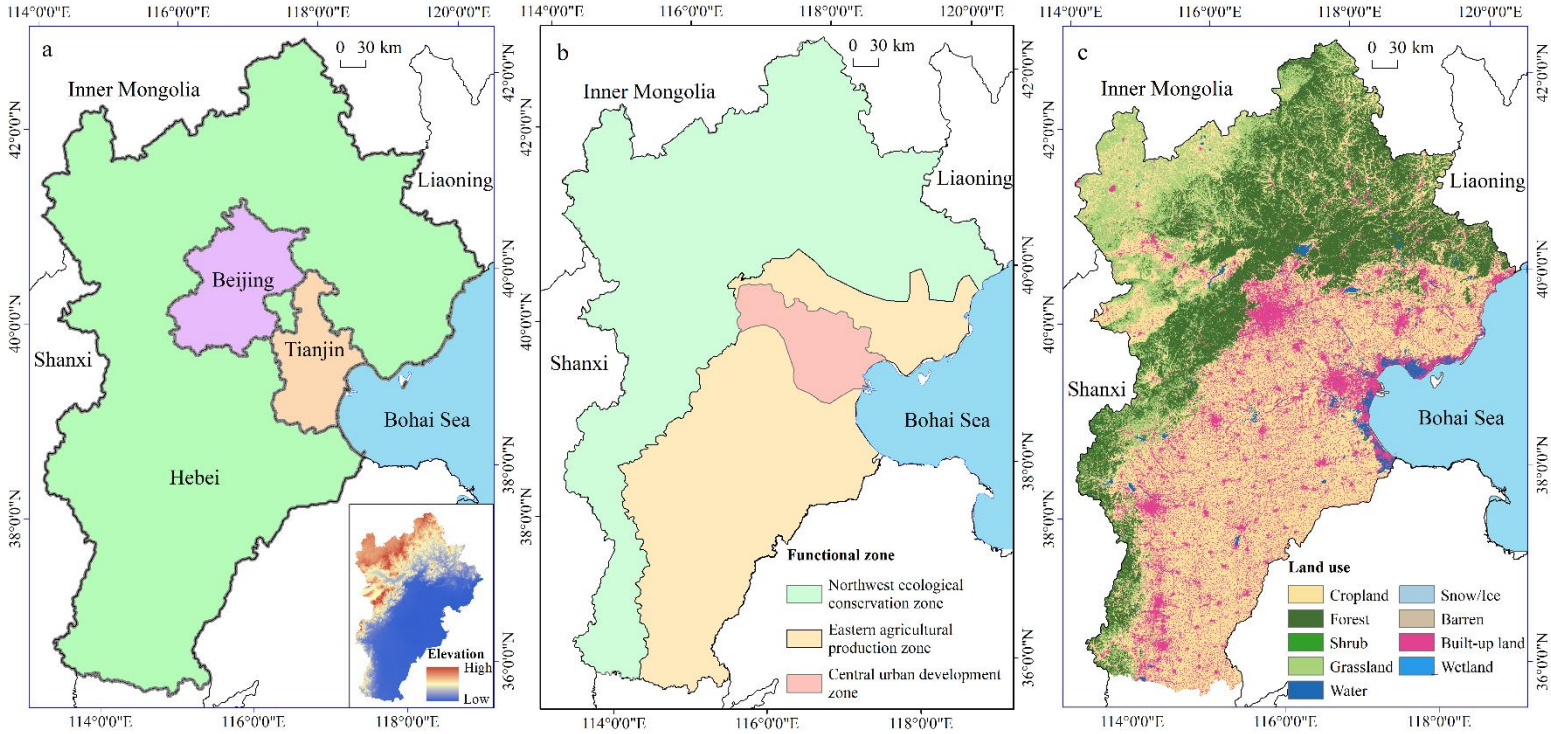


Figure 1. Maps of the BTH region: (a) administrative divisions, (b) functional zones, and (c) land use in 2024.

Since 2000, rapid economic expansion and population growth have intensified demands for ecosystem services such as water conservation, soil retention, and wind erosion prevention (Gao et al., 2024; Li et al., 2022b). However, multiple anthropogenic stressors—including urbanization, intensive cropping, and non-cropping livelihood activities (e.g., grazing, fuelwood collection, and medicinal herb harvesting)—have

increasingly constrained the provision of these services (Li et al., 2018).

2.2 Anthropogenic stressor risk modeling based on BBN

The BBN-based anthropogenic stressor risk modeling involved six steps: variable selection, structure determination, statistical distribution fitting and parameterization, dynamic discretization of nodes, probabilistic inference, and sensitivity analysis, as detailed below.

2.2.1 Model variable selection

Anthropogenic stressor risk is primarily driven by agricultural production, non-cropping livelihood activities, and urbanization, which are influenced by biophysical and socioeconomic indicators at the plot level (IPBES, 2019; Turner et al., 2012). Based on a literature review, ten indicators were selected and categorized into biophysical and socioeconomic groups.

Biophysical indicators capture hydrological conditions, topographic constraints, and resource accessibility. Steeper slopes increase erosion risk (Magdoff and Van Es, 2021). Proximity to surface water can intensify ecological disturbances from agricultural practices, such as fertilizer and pesticide runoff, sediment transport, and eutrophication (Huang and Li, 2025).

Socioeconomic indicators reflect human disturbance and land use pressures. Proximity to roads is associated with higher agricultural production stressors, whereas remote areas generally experience lower stressor levels and maintain higher ecological integrity (Grantham et al., 2020; Shamdasani, 2021). Non-cropping livelihood activities were linked to soil erosion risk in the BBN, which tends to decline with increasing

distance from village (Li et al., 2022a; Li et al., 2024).

Grazing intensity, a key non-cropping activity, is typically represented by livestock numbers (Eldridge et al., 2017). Livestock numbers generally decline with increasing slope gradient (Raynor et al., 2021) and greater distance to village (Pittarello et al., 2021). Furthermore, higher population density and GDP values are linked to greater urbanization pressures (Seto et al., 2012). These socioeconomic indicators are strongly associated with distance to township (Liu et al., 2014) and county (Zhou et al., 2011). The datasets used in this study, including their spatial resolution, format, and sources, are summarized in Table 1.

Table 1. Datasets used in this study and their key information

Dataset	Year	Temporal resolution	Spatial resolution	Format	Source
The 30 m annual land cover datasets and its dynamics in China from 1985 to 2024	2000, 2024	1 year	30 m	GeoTiff	(Yang and Huang, 2024)
The Global Roads Inventory Project dataset	2018	1 year	N/A	Shapefile	(Meijer et al., 2018)
China-LDRL: China's surface water bodies, large dams, reservoirs, and lakes dataset	2019	1 year	N/A	Shapefile	(Wang et al., 2022)
Global Pasture Watch - Annual livestock headcount maps for cattle, goats, sheep and horses at 1-km 2000 – 2022 (FAOSTAT-adjusted) (v1)	2022	1 year	1 km	GeoTiff	(Parente et al., 2025)
90 m digital elevation database v4.1	2008	1 year	90 m	GeoTiff	(Jarvis et al., 2008)
Dataset of soil erosion intensity in 20 countries in key regions (five levels, high intensity ≥ 3)	2015	1 year	300 m	GeoTiff	(Zhang, 2021)
National statistical area and urban-rural classification codes	2020	1 year	N/A	csv	(National Bureau of Statistics, 2020)
The population density in 2022	2022	1 year	30 arc-sec	GeoTiff	(Liu et al., 2024)
The total GDP at purchasing power parity in 2020	2020	1 year	30 arc-sec	GeoTiff	(Kummu et al., 2025)

All gridded datasets were reprojected to an Albers Equal Area projection based on the WGS 1984 datum, resampled to 1 km resolution to balance accuracy and computational efficiency, and masked to a common extent. Slope gradient was derived from the digital elevation model using ArcGIS 10.4.1. The geographic coordinates of villages, townships, and counties were converted to shapefiles, which, together with road and surface water datasets, were used to calculate the distance to the nearest road, surface water, village, township, and county using the terra, sf, and dplyr packages in R.

2.2.2 Model structure determination

The BBN structure was developed based on the interrelationships among plot-level indicators, anthropogenic stressors, and ecological risk, as represented by stressor risk (Figure 2).

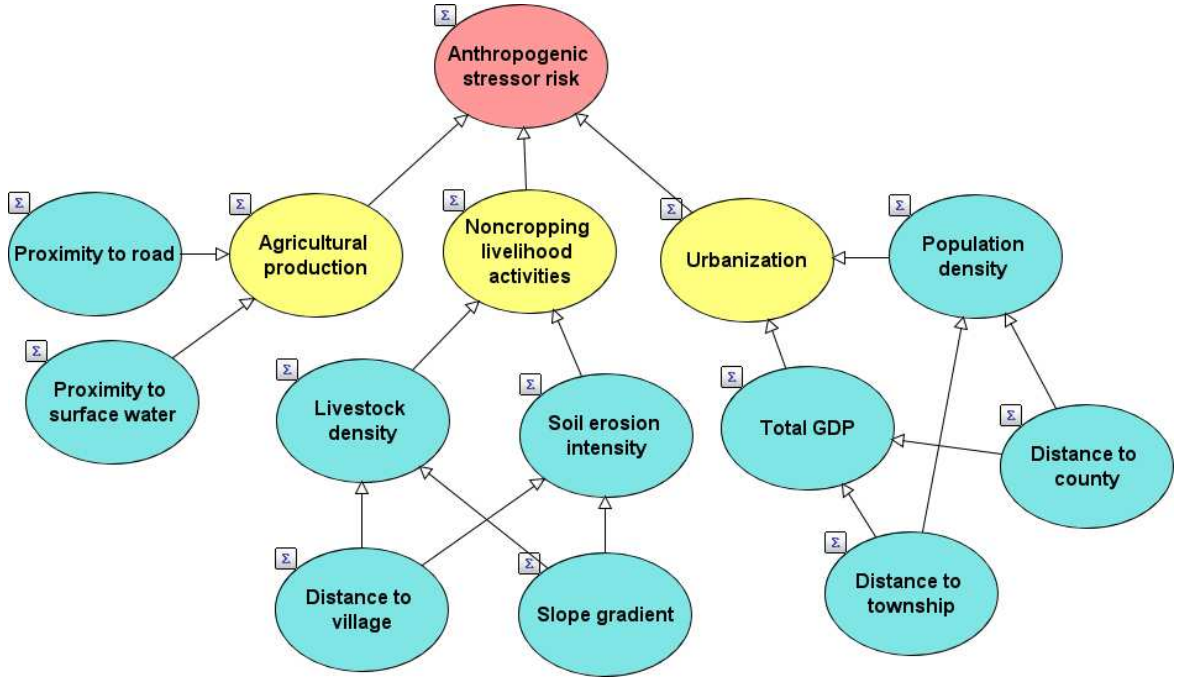


Figure 2. Structure of the BBN showing cumulative anthropogenic stressor risk (red), individual anthropogenic stressor risks (yellow), and plot-level indicators (blue).

In the network, the three tiers are distinguished by color, and directed arcs denote causal

dependencies, while their absence indicates conditional independence (Borsuk et al., 2006). Accordingly, the joint probability distribution P(X) can be factorized as:

$$P(X) = P(x_1, \dots, x_n) = \prod_{i=1}^{n} P(x_i|\pi_i) \quad (1)$$

where π_i represents the parent nodes of variable x_i. This conditional independence substantially reduces computational complexity (Poole and Zhang, 2003). To identify anthropogenic stressors, we analyzed land use changes from 2000 to 2024 (Table 2). For each plot, the presence of a stressor was assigned a value of 1, and its absence a value of 0.

Table 2. Anthropogenic stressors associated with land use changes (2000–2024)

Anthropogenic stressor	Land use in 2000	Land use in 2024
Agricultural production	Forest, shrub, grassland, water, snow/ice, barren land, built-up land, wetland	Farmland
Non-cropping livelihood activity	Forest	Shrub, grassland, barren land
	Shrub	Grassland, barren land
	Grassland	Barren land
	Cropland	Barren land
Urbanization	Cropland, forest, shrub, grassland, water, snow/ice, barren land, wetland	Built-up land

Agricultural production and urbanization correspond to land conversion into cropland and built-up land, respectively. In contrast, non-cropping livelihood activities drive local land degradation (Li et al., 2021), whereby land uses with higher primary productivity (e.g., forest) are converted into those with lower productivity (e.g., shrub, grassland, barren land). If at least one of the three stressors occurred on a plot, the anthropogenic stressor risk was assigned a value of 1; otherwise, it was set to 0. The spatial distributions of the gridded node

188 layers are shown in Figure S1, including the cumulative stressor, three individual stressors,
189 and all plot-level indicators.
190 Finally, all layers were integrated into a unified attribute database (212,177 plots) for
191 dynamic discretization in R.
192 **2.2.3 Statistical distribution fitting and parameterization**
193 We fitted candidate statistical distributions to all node variables. Discrete nodes (Figures
194 S1(a)–10(e)) were evaluated with Poisson, Binomial, and Multinomial distributions,
195 whereas continuous nodes (Figures S1(f)–10(n)) were tested against Normal, LogNormal,
196 Gamma, and Weibull distributions. Model selection followed established goodness-of-fit
197 procedures (Delignette-Muller and Dutang, 2015). For continuous variables, model fit was
198 assessed using the Akaike Information Criterion (AIC), Bayesian Information Criterion
199 (BIC), and the Kolmogorov–Smirnov (KS) test. For discrete variables, model choice was
200 based primarily on AIC and BIC, as KS-type statistics are less informative for categorical
201 data. The best-fitting distributions were then parameterized using appropriate data-driven
202 estimation techniques, including maximum likelihood, method-of-moments, and
203 regression-based approaches, with detailed procedures and estimates provided in the
204 Appendix A.
205 **2.2.4 Dynamic discretization of nodes**
206 Continuous variables were discretized to facilitate conditional probability table (CPT)
207 specification and improve computational efficiency in the BBN (Nojavan A et al., 2017).
208 Among various approaches, we adopted the dynamic discretization algorithm (Fenton and
209 Neil, 2018), which partitions continuous variables into intervals by minimizing the

Kullback–Leibler divergence between continuous and discrete distributions. The algorithm iteratively refines the discretization until convergence and dynamically updates intervals in response to new evidence, thereby ensuring accurate representation of continuous variables while maintaining computational efficiency and reliability during inference.

Based on the causal dependencies among nodes (Figure 2), the best-fitting distributions and discretized variables were parameterized to construct CPTs. Conditional probabilities for discrete nodes were estimated using multinomial logistic regression, with predictor variables (e.g., agricultural production) determined by their parent nodes (e.g., proximity to road, proximity to surface water). For continuous nodes, distribution parameters were derived either directly from the unified attribute database (for parent nodes) or estimated through regression modeling conditioned on their parent nodes (for child nodes). To balance computational efficiency and model accuracy, the maximum number of iterations and the convergence threshold for parameter estimation were set to 50 and 0.001, respectively (Fenton and Neil, 2018).

2.2.5 Probabilistic inference

Once the network structure and parameters were defined, the BBN functioned as a probabilistic expert system, supporting reasoning under uncertainty through Bayesian updating and evidence propagation. In this study, predictive inference was applied by conditioning the network on observed plot-level indicator data to infer downstream stressor and cumulative risk outcomes, allowing posterior probability distributions to be estimated and mapped across the study area.

2.2.6 Sensitivity analysis

Sensitivity analysis was conducted to identify the key drivers of cumulative stressor risk by varying the probability distribution of one input node at a time while holding others constant (Marcot, 2006; Pollino et al., 2007). The expected information gain, measured as entropy reduction between the target variable Q (cumulative stressor risk) and an input variable F, is given by:

$$I(Q;F) = H(Q) - H(Q|F) = \sum_q \sum_f P(q,f) \log_2 \frac{P(q,f)}{P(q)P(f)} \quad (2)$$

where q and f index the states of Q and F, P(q, f) is their joint probability, and $H(Q)=-\sum_q P(q)\log_2 P(q)$ is the Shannon entropy of Q. A larger I(Q; F) indicates that F has a stronger influence on Q by reducing uncertainty. All sensitivity analyses and probabilistic inferences were implemented using Agena.ai Modeller and its R API (agena.ai package).

2.3 GWR and multiscale GWR (MGWR)

To explore the spatial heterogeneity of driving mechanisms underlying anthropogenic stressor risk patterns, GWR and MGWR were employed following the global ordinary least squares (OLS) analysis. Prior to local modeling, multicollinearity among explanatory variables was assessed separately for anthropogenic stressor nodes and plot-level indicator nodes using variance inflation factors (VIFs) based on global OLS models (Dormann et al., 2012). Variables with VIF values < 10 were considered to exhibit acceptable collinearity. All continuous variables were standardized (z-score transformation) prior to analysis to ensure the comparability of regression coefficients and to improve numerical stability.

2.3.1 GWR

GWR extends the conventional OLS framework by allowing regression coefficients to vary continuously over space, thereby capturing spatial non-stationarity in relationships between

the dependent variable and explanatory factors (Fotheringham, 2008). The basic form of the GWR model can be expressed as:

$$y_i = \beta_0(u_i, v_i) + \sum_{k=1}^{p} \beta_k (u_i, v_i) x_{ik} + \varepsilon_i \quad (3)$$

where y_i denotes the anthropogenic stressor risk value at location i; x_{ik} is the k-th explanatory variable; (u_i, v_i) represents the spatial coordinates of location i; $\beta_k(u_i, v_i)$ are location-specific regression coefficients; and ε_i is the random error term.

Local parameter estimates are obtained through weighted least squares, in which observations closer to location i are assigned higher weights according to a spatial kernel function. In this study, a fixed bisquare kernel was adopted, and the optimal bandwidth was selected by minimizing the corrected Akaike Information Criterion (AICc). Comparisons between OLS and GWR model performance (AICc and R^2) were used to evaluate the presence of spatial non-stationarity in risk drivers.

2.3.2 MGWR

While conventional GWR assumes that all explanatory variables operate at a single spatial scale, this assumption may be overly restrictive for complex socio-ecological systems. MGWR relaxes this constraint by allowing each explanatory variable to be associated with its own optimal bandwidth, thereby explicitly capturing multiscale processes (Fotheringham et al., 2017). The MGWR model is formulated as:

$$y_i = \beta_0(u_i, v_i) + \sum_{k=1}^{p} \beta_k^{(bw_k)} (u_i, v_i) x_{ik} + \varepsilon_i \quad (4)$$

where bw_k denotes the optimal bandwidth associated with the k-th explanatory variable. Smaller bandwidths indicate localized effects, whereas larger bandwidths suggest more spatially homogeneous or global-scale influences.

In this study, MGWR was applied separately to anthropogenic stressor nodes and plot-level

277 indicator nodes to disentangle their respective spatial scales and effect heterogeneity. Model
278 calibration followed an iterative back-fitting procedure, and bandwidths for individual
279 coefficients were optimized using AICc minimization (Fotheringham et al., 2017; Lu et al.,
280 2018). Model performance relative to OLS and GWR was evaluated using AICc and the
281 coefficient of determination (R^2). The GWR and MGWR analyses were implemented using
282 the GWmodel package in R (Gollini et al., 2015).
283 A schematic of the overall technical workflow is presented in Figure 3.

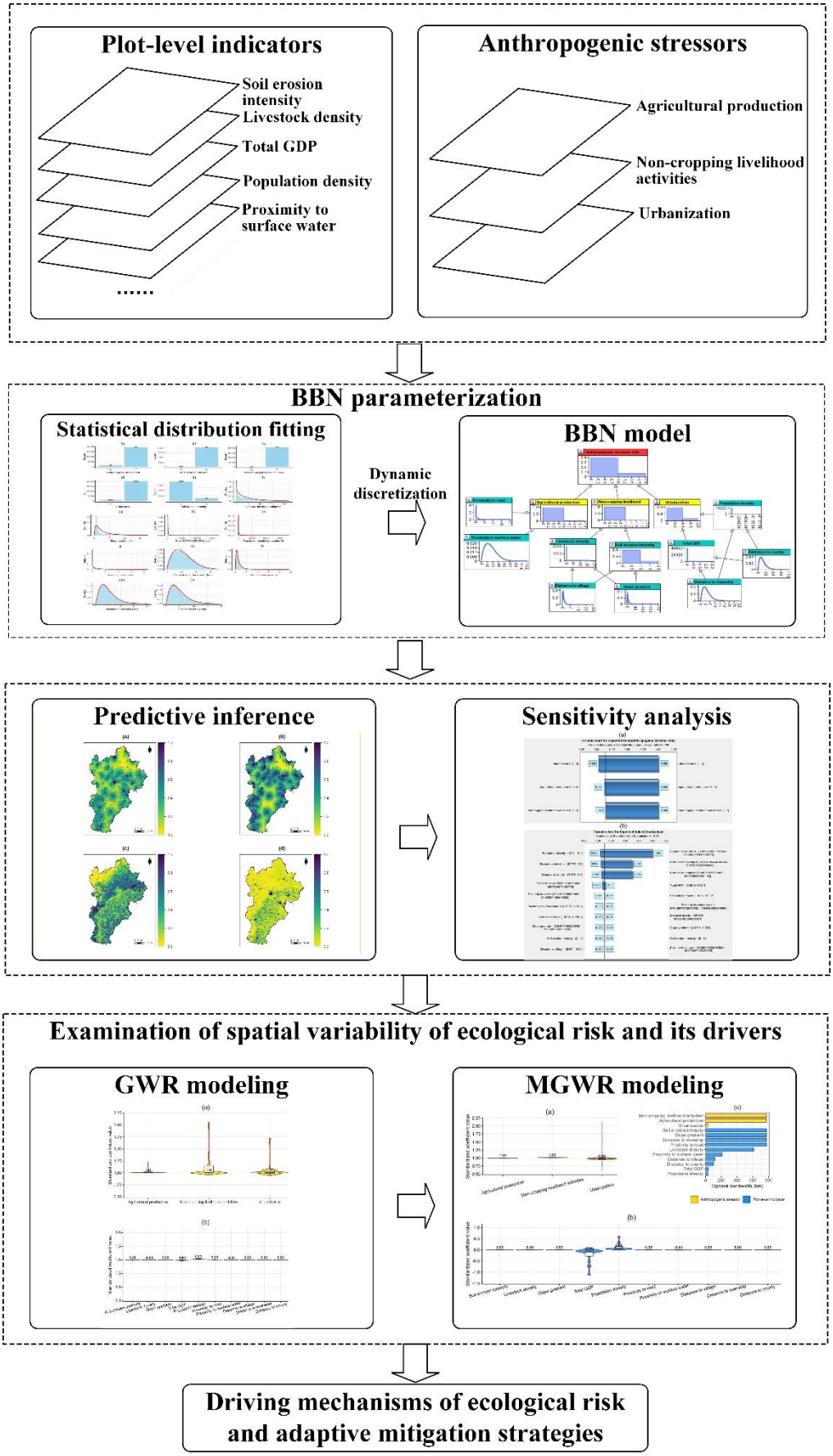


Figure 3. Technical workflow

3. Results

3.1 Land use change dynamics

Sankey diagrams were used to examine land use change dynamics in the BTH region and its three functional zones from 2000 to 2024 (Figure 4).

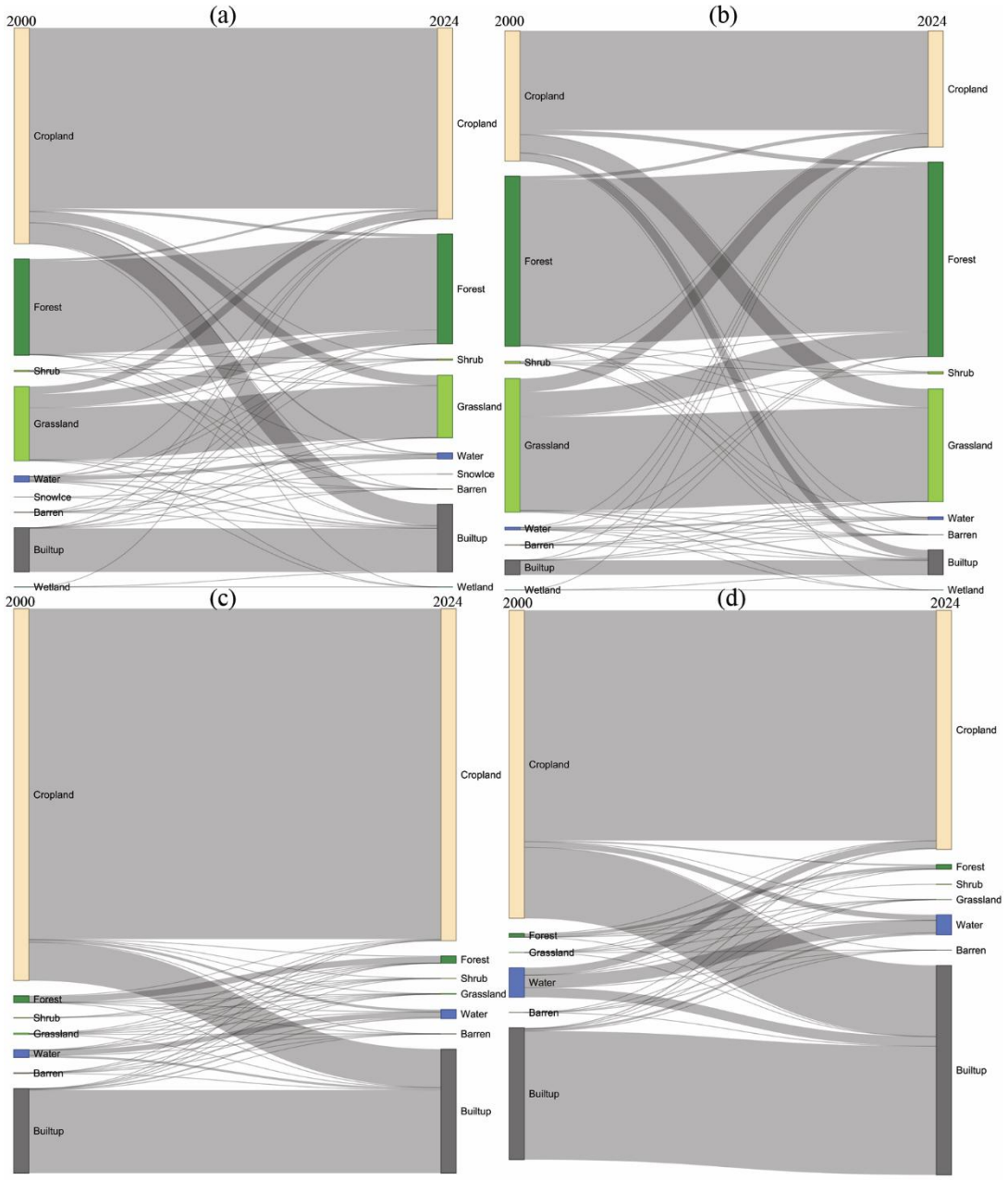


Figure 4. Land use change dynamics of the BTH region and its three functional zones from 2000 to 2024, illustrated using Sankey diagrams. (a) BTH region; (b) Northwest ecological conservation zone; (c) Eastern agricultural production zone; (d) Central urban development zone.

Overall, the BTH region is dominated by cropland, forest, grassland, and built-up land (Figure 4(a)). The northwest ecological conservation zone generally exhibits a similar land use composition (Figure 4(b)). In this zone, cropland remained relatively stable over the period 2000–2024, whereas forest and built-up land increased markedly, primarily at the expense of grassland and, to a lesser extent, cropland. Although limited conversion from cropland partially compensated for grassland losses, grassland experienced a pronounced net decline due to substantial outflows to both forest and cropland.

The eastern agricultural production zone and the central urban development zone, both dominated by cropland and built-up land, display broadly similar land use dynamics (Figure 4(c)–4(d)). In these zones, cropland decreased substantially while built-up land expanded markedly, driven mainly by extensive conversion from cropland to built-up land. Consequently, at the scale of the entire BTH region, cropland and grassland show significant net decreases, whereas forest and built-up land exhibit pronounced increases over this period (Figure 4(a)).

3.2 Statistical distribution fitting

We evaluated the goodness-of-fit of candidate statistical distributions for both continuous and discrete variables. Detailed results for all candidate distributions are provided in Tables S1 and S2. For continuous variables, a lower AIC/BIC and, in principle, a non-significant KS test result ($p \geq 0.05$) indicate a better model fit. For discrete variables, the best-fitting distribution was selected as the one with the lowest AIC and BIC values among the candidate models, as KS-type tests are not informative for categorical data. The final best-fitting distributions for all variables are summarized in Table 3.

Table 3. Goodness-of-fit statistics for continuous and discrete variables under the best-fitting statistical distributions. For continuous variables, KS p-value indicates the significance level of the Kolmogorov–Smirnov test (* $p < 0.05$). NA indicates not applicable for discrete variables.

Type	Variable	Best-fitting distribution	AIC	BIC	KS statistic	KS p-value
Discrete	Anthropogenic stressor risk	Multinomial	13.5	23.8	NA	NA
Discrete	Agricultural production	Multinomial	12.3	22.6	NA	NA
Discrete	Non-cropping livelihood activities	Multinomial	10.1	20.4	NA	NA
Discrete	Urbanization	Multinomial	13.1	23.4	NA	NA
Discrete	Soil erosion intensity	Multinomial	13.9	24.1	NA	NA
Continuous	Livestock density	Weibull	1927315.6	1927335.94	0.082	*
Continuous	Slope gradient	LogNormal	-252267	-252246	0.114	*
Continuous	Total GDP	Weibull	905357.5	905377.78	0.063	*
Continuous	Population density	LogNormal	2475609.5	2475629.7	0.081	*
Continuous	Proximity to road	Gamma	3676657.8	3676678.30	0.006	*
Continuous	Proximity to surface water	Weibull	4689840.3	4689860.84	0.019	*
Continuous	Distance to village	LogNormal	3516909.9	3516930.38	0.025	*
Continuous	Distance to township	Gamma	3943461.2	3943481.73	0.009	*
Continuous	Distance to county	Gamma	4530591.8	4530612.37	0.016	*

Due to the large sample size, the KS test yielded significant results ($p < 0.05$) for continuous variables, a well-known limitation of goodness-of-fit tests under big data conditions

(Delignette-Muller and Dutang, 2015). Therefore, model selection relied mainly on relative AIC/BIC values and visual assessment of fit. Visual fitting results are presented in Figure 5, indicating satisfactory fit for all variables.

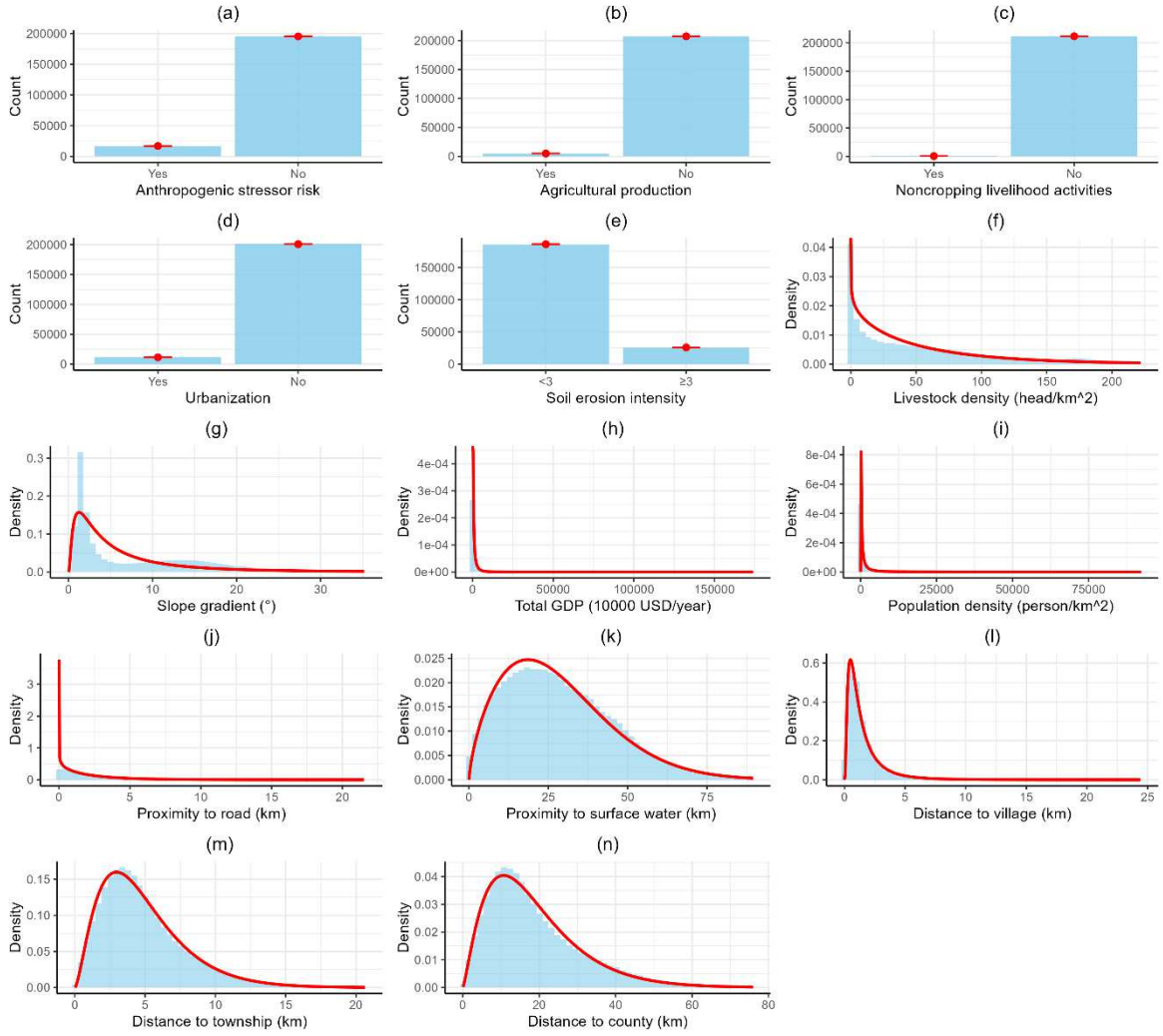


Figure 5. Visual assessment of best-fitting distributions for discrete and continuous variables

Based on the unified attribute database, the estimated parameters of the best-fitting distributions for both discrete and continuous variables are summarized in Table 4.

Table 4. Estimated parameters of best-fitting distributions for discrete and continuous variables. Regression-based functional forms are provided where applicable.

Type	Variable	Best-fitting distribution	Parameters / Regression form
Discrete	Anthropogenic stressor risk	Multinomial (logit)	P(agricultural_production) + P(non-cropping_livelihood_activities) + P(urbanization)
Discrete	Agricultural production	Multinomial (logit)	$1 / (1 + \exp(3.35 + 0.02 \times \text{proximity_surface_water} - 0.07 \times \text{proximity_to_road}))$
Discrete	Non-cropping livelihood activities	Multinomial (logit)	$1 / (1 + \exp(5.48 + 0.02 \times \text{livestock_density} - 0.42 \times \text{soil_erosion_intensity}))$
Discrete	Urbanization	Multinomial (logit)	$1 / (1 + \exp(2.96 + 6.88 \times 10^{-5} \times \text{total_GDP} - 2.07 \times 10^{-4} \times \text{population_density}))$
Discrete	Soil erosion intensity	Multinomial (logit)	$1 / (1 + \exp(1.94 + 0.31 \times \text{distance_to_village} - 0.05 \times \text{slope_gradient}))$
Continuous	Livestock density	Weibull	Shape = 0.4; Scale = 34.7 + 0.17 × distance_to_village − 0.06 × slope_gradient
Continuous	Total GDP	Weibull	Shape = 0.3; Scale = 2533.29 − 0.09 × distance_to_county − 0.45 × distance_to_township
Continuous	Proximity to surface water	Weibull	Shape = 1.69; Scale = 31.52
Continuous	Slope gradient	LogNormal	Mean = 1.44; Standard deviation = 1.11
Continuous	Population	LogNormal	Mean = log(1516.54 − 24.24 × distance_to_county − 106.25 × distance_to_township);

Type	Variable	Best-fitting distribution	Parameters / Regression form
	density		Standard deviation = 2.52
Continuous	Distance to village	LogNormal	Mean = 0.08; Standard deviation = 0.89
Continuous	Proximity to road	Gamma	$\alpha = 0.81$; $\beta = 2.66$
Continuous	Distance to township	Gamma	$\alpha = 2.64$; $\beta = 1.84$
Continuous	Distance to county	Gamma	$\alpha = 2.37$; $\beta = 7.9$

326

These distribution parameters provided the basis for dynamic discretization and construction of the CPTs. The resulting parameterization process is described in Section 3.2.

3.2 BBN parameterization

Based on dynamic discretization, the fully parameterized BBN model was derived (Figure 6).

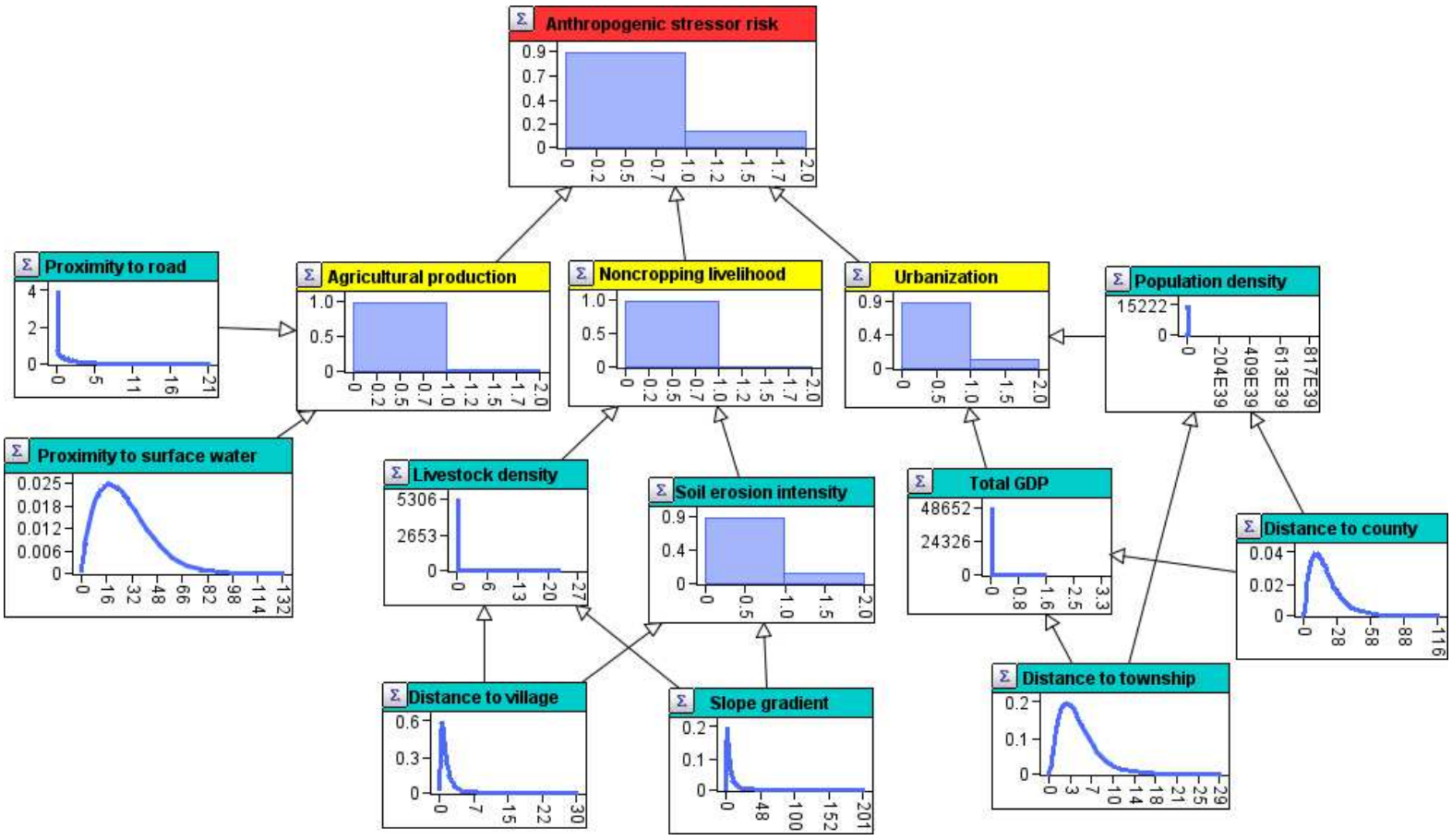
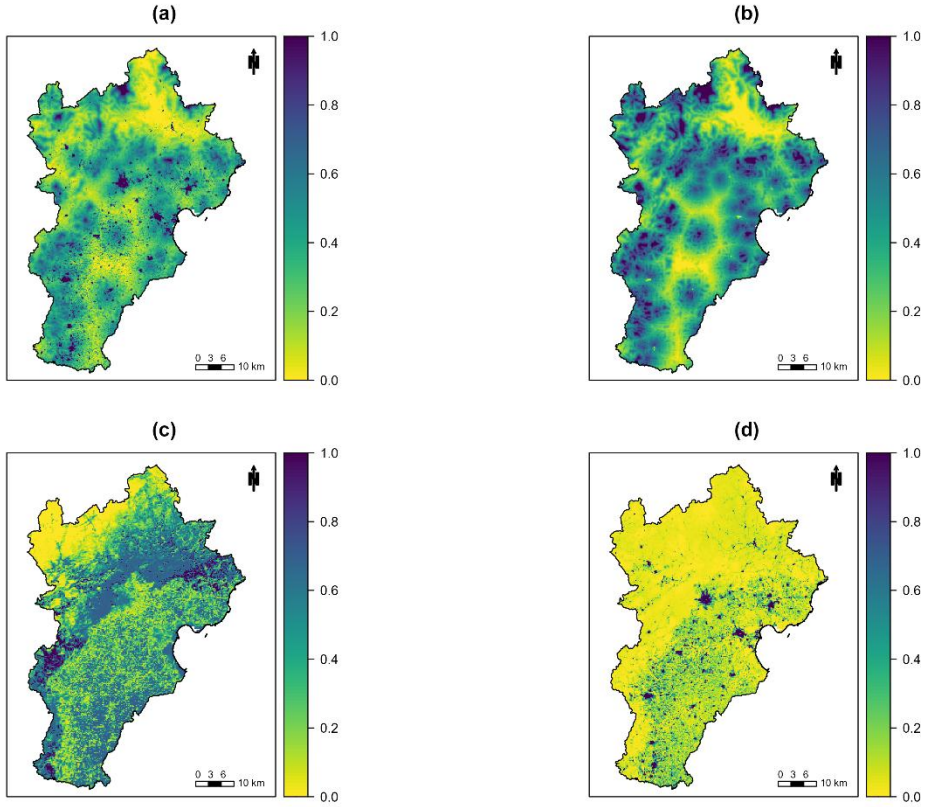


Figure 6. Parameterized BBN model showing nodes, dependencies, and estimated CPTs.

3.3 Spatial patterns of individual and cumulative anthropogenic stressor risks

Based on predictive inference under future scenarios, Figure 7 illustrates the spatial patterns of three individual anthropogenic stressor risks and their cumulative risk across the BTH region.



337 Figure 7. Spatial patterns of predicted risks from three anthropogenic stressors and their cumulative risk
338 across the BTH region. (a) Cumulative anthropogenic stressor risk; (b) Agricultural production risk; (c)
339 Non-cropping livelihood activity risk; (d) Urbanization risk.

340 The predicted risk associated with agricultural production exhibits extensive high-risk
341 clusters throughout the region (Figure 7(b)). In contrast, the risk from non-cropping
342 livelihood activities is primarily concentrated in the northwestern mountainous areas, while
343 appearing more fragmented across the southeastern plains (Figure 7(c)). Urbanization risk
344 is strongly concentrated around major cities, particularly Beijing and Tianjin (Figure 7(d)).
345 The spatial superposition of these future stressor risks generates a pronounced gradient in
346 cumulative risk across the BTH region, characterized by clear spatial agglomeration patterns
347 (Figure 7(a)). These spatially clustered high-risk areas highlight priority areas for
348 conservation and risk mitigation, where targeted management of dominant stressors could

yield disproportionate benefits for reducing cumulative stressor risk.

3.4 Spatial-scale variations in individual and cumulative anthropogenic stressor risks

Figure 8 presents the Spearman rank correlations of individual and cumulative anthropogenic stressor risks across different spatial scales.

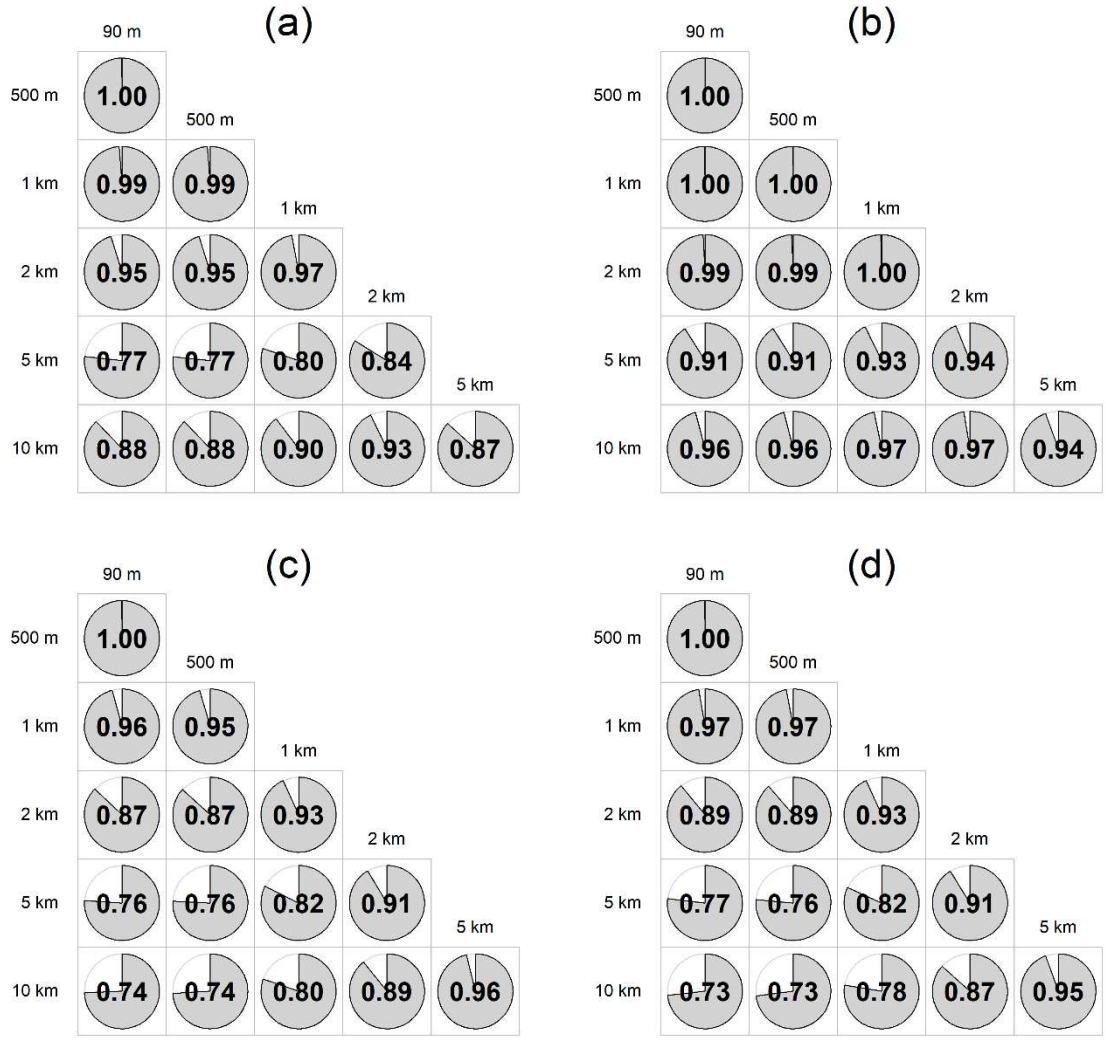


Figure 8. Spearman rank correlation matrices of predicted risks from three specific anthropogenic stressors and their cumulative risk across different spatial scales. (a) Cumulative anthropogenic stressor risk; (b) Agricultural production risk; (c) Non-cropping livelihood activity risk; (d) Urbanization risk.

Agricultural production risk exhibits consistently high correlations across spatial scales (Spearman's $\rho \geq 0.91$), indicating stable spatial patterns (Figure 8(b)). In contrast, non-

358 cropping livelihood activity and urbanization risks show greater spatial divergence, as
359 reflected by lower cross-scale correlations, particularly between finer (90 m and 500 m) and
360 coarser (5 km and 10 km) resolutions (Spearman's $\rho \leq 0.77$; Figure 8(c)–8(d)). Consequently,
361 Spearman correlations of the cumulative risk exhibit a moderate decline with increasing
362 disparities in spatial resolution ($\rho \leq 0.88$; Figure 8(a)).

363 **3.5 Sensitivity analysis**

364 The results of sensitivity analysis are presented as tornado diagrams (Figure 9).

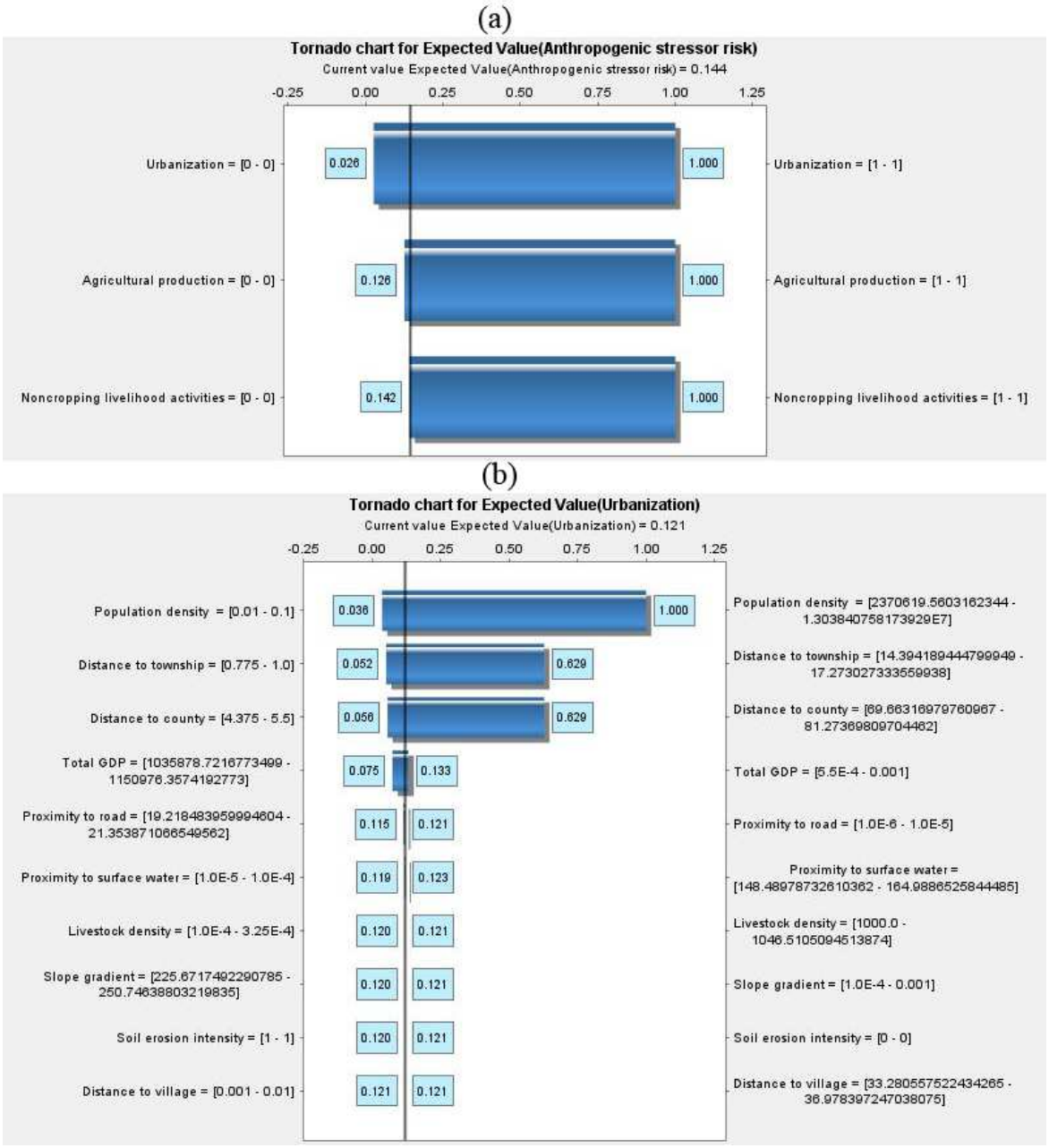


Figure 9. Sensitivity analysis of anthropogenic stressor – tier and plot-level indicator – tier nodes, quantified by entropy reduction. (a) Anthropogenic stressor tier; (b) Plot-level indicator tier.

At the anthropogenic stressor tier, changing the state of urbanization from 0 (non-occurrence) to 1 (occurrence) increased the probability of cumulative stressor risk from 0.026 to 1, resulting in the largest entropy reduction (0.974; blue bar). This indicates that the occurrence likelihood of urbanization stressor exerts the strongest influence on future cumulative risk. The remaining stressors showed slightly lower but comparable sensitivities, ranked as

agricultural production occurrence (0.874) and non-cropping livelihood activity occurrence (0.858) (Figure 9(a)).

At the plot-indicator tier, population density exhibited the highest sensitivity (0.964), followed by distance to township (0.577) and distance to county (0.573). These indicators are primarily associated with urbanization-related processes. All remaining indicators showed entropy reductions below 0.1, indicating relatively limited influence on cumulative stressor risk (Figure 9(b)).

Subsequently, the BBN was reparameterized for the three functional zones to examine spatial variations in sensitivity across two tiers of nodes (Figure 10).

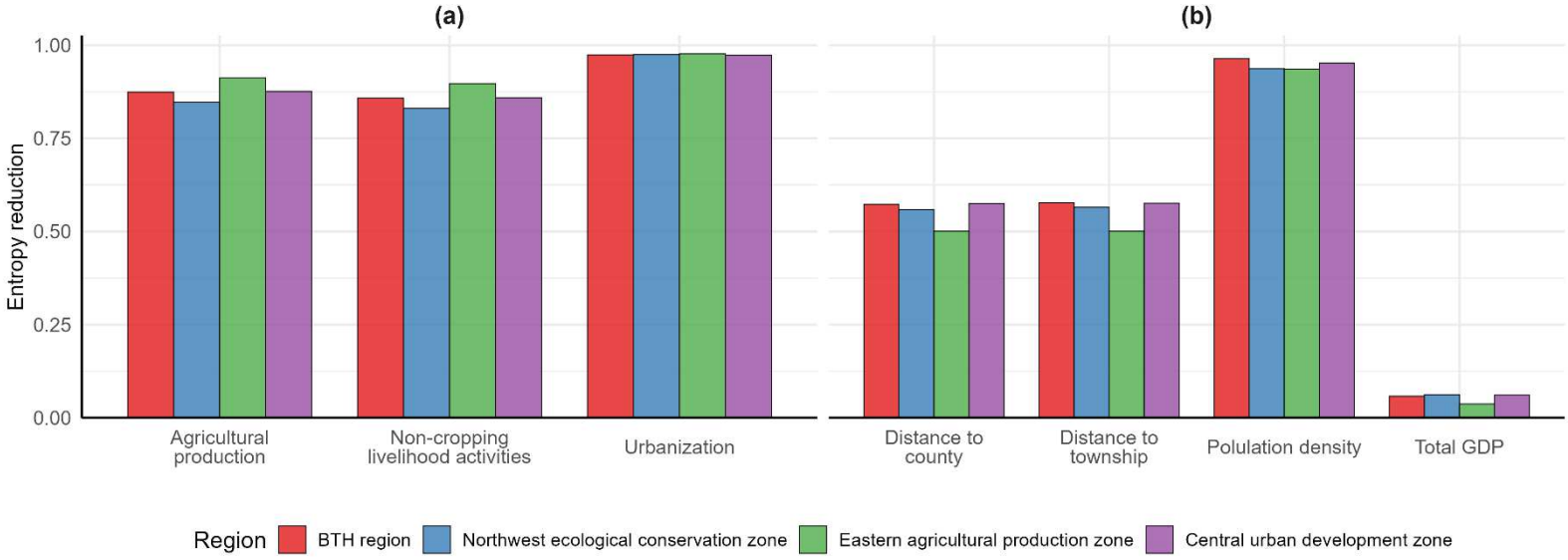


Figure 10. Spatial variations in sensitivity across two tiers of BBN nodes among functional zones. (a) Anthropogenic stressor tier; (b) Plot-level indicator tier.

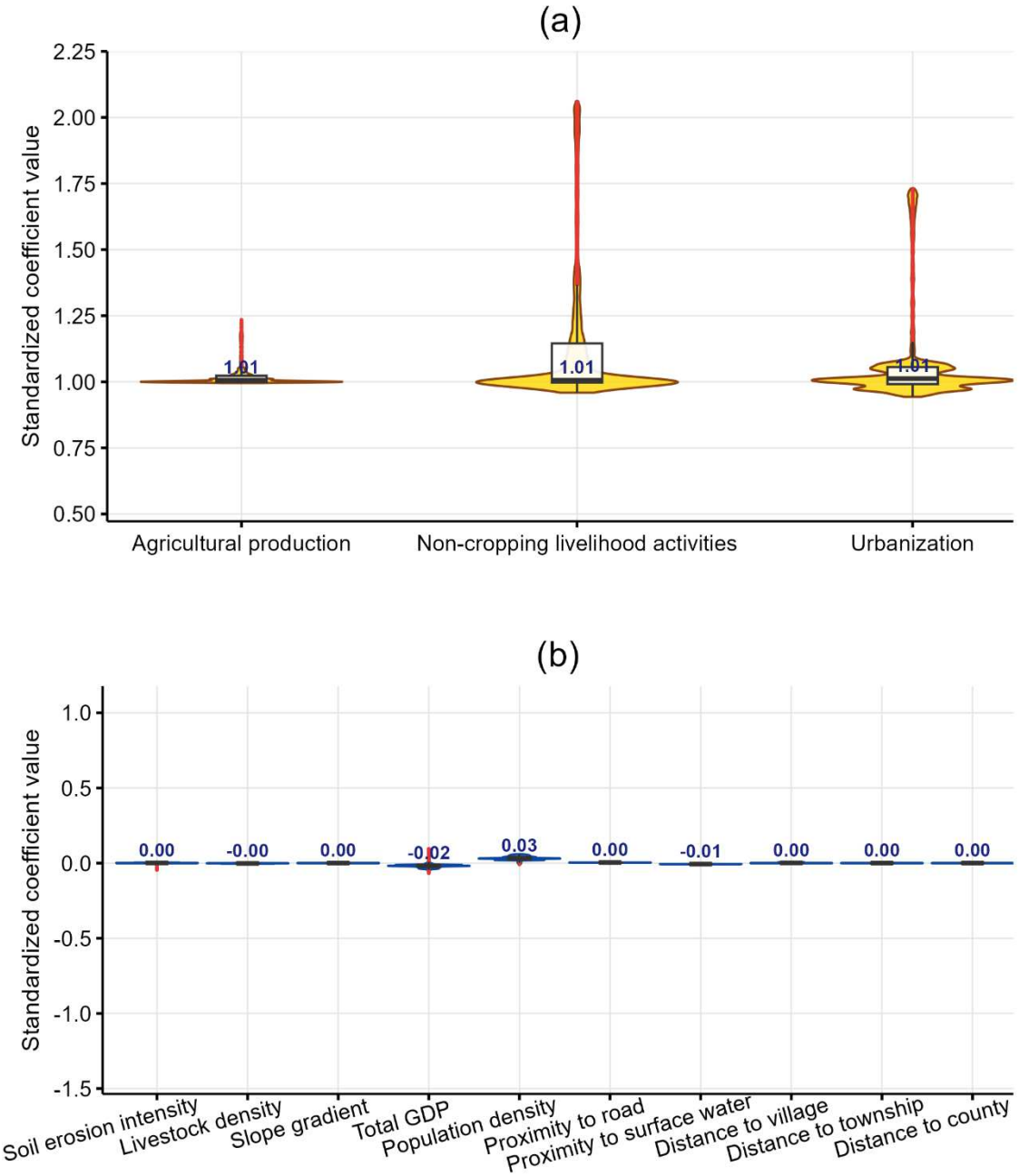
Overall, the three functional zones exhibit sensitivity patterns broadly consistent with those observed for the entire BTH region at both node tiers. However, the eastern agricultural production zone shows a distinct magnitude of variation. In this zone, sensitivities associated with agricultural production risk and non-cropping livelihood activity risk are

markedly higher than those in the other zones and in the BTH region as a whole (Figure 10(a)). In contrast, sensitivities related to distance to county, distance to township, and total GDP are substantially lower (Figure 10(b)). These results indicate that the eastern agricultural production zone is particularly responsive to agricultural production- and non-cropping livelihood activity-related risks, while exhibiting relatively weaker sensitivity to urbanization-related indicators.

3.6 Spatial variations of anthropogenic stressor risk drivers

All model nodes exhibit VIF values well below the commonly accepted threshold of 10, indicating no severe multicollinearity among anthropogenic stressor nodes and plot-level indicator nodes (Figure S2). Subsequently, the GWR for all the BNN nodes was conducted. Compared with the global OLS models, the GWR models exhibited notably better model fit for both groups of predictors. For anthropogenic stressors, the coefficient of determination (R^2) increased from 0.817 in the OLS model to 0.84 in the GWR model, accompanied by a clear reduction in AICc (from −66,613 to −67,999). For plot-level indicators, model performance improved more substantially, with R^2 increasing from 0.864 to 0.9 and AICc decreasing from −69,749 to −72,913. These consistent improvements in explanatory power and model parsimony suggest that allowing regression coefficients to vary spatially captures important spatial heterogeneity that is not adequately represented by global models, providing strong evidence for spatial non-stationarity in the relationships between cumulative anthropogenic stressor risk and its drivers.

The distributions of local GWR coefficients for the BBN nodes were illustrated using violin and box plots (Figure 11).



409 Figure 11. Distributions of local GWR coefficients for the BBN nodes. (a) Anthropogenic stressor nodes;

410 (b) Plot-level indicator nodes.

411 At the regional scale, anthropogenic stressor nodes exhibit pronounced spatial heterogeneity

412 in their local associations with cumulative stressor risk, as evidenced by broad coefficient

413 ranges and asymmetric distribution shapes across the three stressors (Figure 11(a)). Among

414 them, non-cropping livelihood activities and urbanization display wider interquartile ranges
415 and more elongated distribution tails. In contrast, the agricultural production shows
416 comparatively narrower interquartile ranges and shorter tails. Although the degrees of
417 spatial heterogeneity differ among stressors, their median coefficient values are broadly
418 comparable, implying that anthropogenic stressors exert similar overall levels of influence
419 on the risk.
420 Compared with stressor nodes, plot-level indicator nodes generally exhibit more
421 concentrated coefficient distributions, with the exception of soil erosion intensity, total GDP,
422 and population density (Figure 11(b)). Most indicator nodes show relatively small
423 coefficient magnitudes, whereas total GDP and population density display notably greater
424 variability, reflecting differences in the strength and spatial consistency of their local
425 relationships with the risk.
426 While GWR accounts for spatial non-stationarity, it imposes a common spatial scale across
427 all predictors. The contrasting behaviors between stressor and indicator nodes therefore
428 motivate further examination of whether these drivers operate at distinct spatial scales,
429 which is addressed using MGWR (Figure 12).

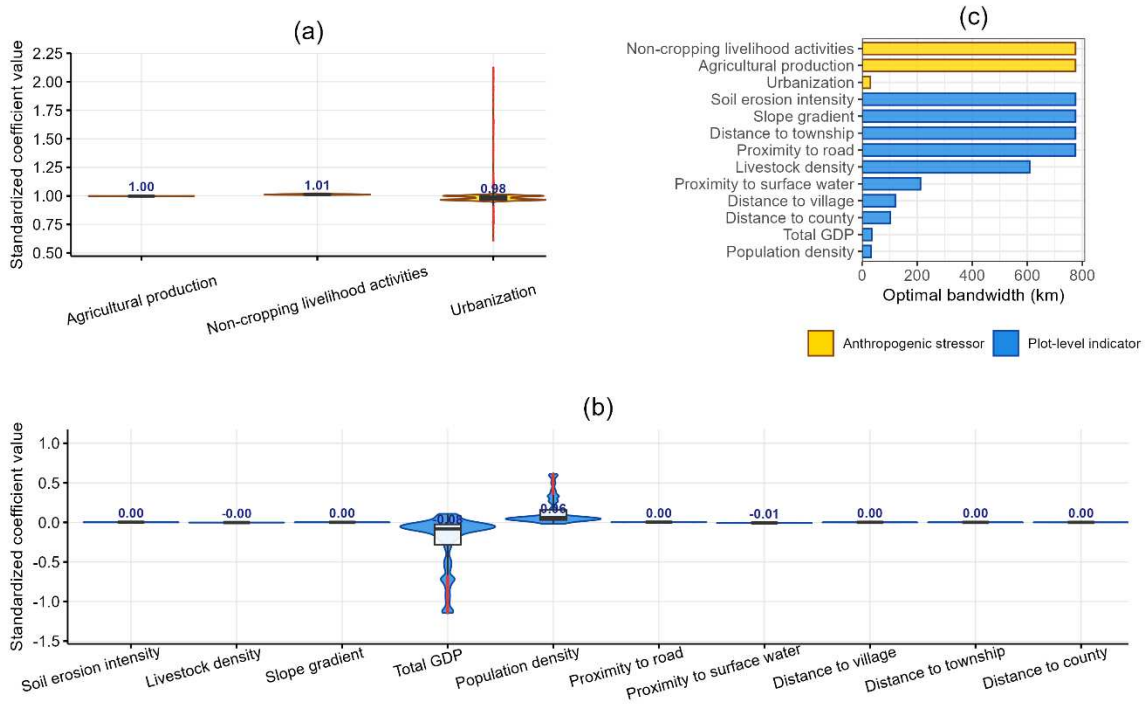


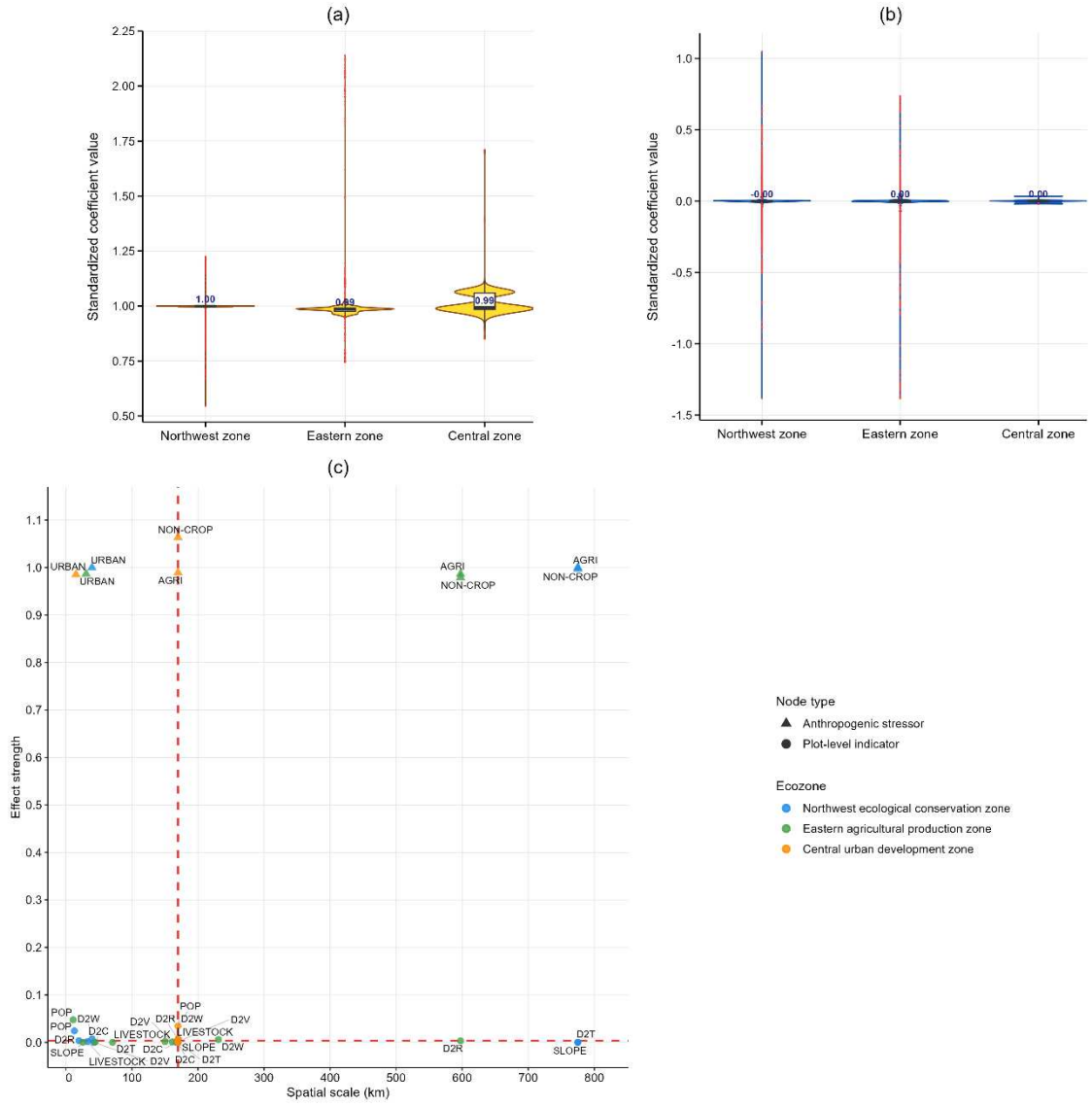
Figure 12. Distributions of local MGWR coefficients and optimal bandwidths for the BBN nodes. (a) Anthropogenic stressor nodes; (b) Plot-level indicator nodes; (c) Optimal bandwidths of the BBN nodes.

For anthropogenic stressor nodes, MGWR produces more concentrated coefficient distributions with fewer extreme values than GWR, except for urbanization (Figure 12(a)). A similar stabilization is observed for most plot-level indicator nodes, with the exception of total GDP and population density, as indicated by narrower interquartile ranges and more compact distributions (Figure 12(b)). These patterns suggest reduced local coefficient uncertainty and more robust spatial estimation under MGWR. In terms of optimal MGWR bandwidths, most coefficients are associated with very large bandwidths (>600 km), whereas urbanization, GDP, population density, and distance-related indicators for surface water, villages, and counties exhibit substantially smaller bandwidths (≤ 212 km), indicating clear contrasts in the spatial scales at which different drivers influence risk (Figure 12(c)).

Building on the regional-scale patterns identified in Figure 12, the distributions of local

coefficients and optimal bandwidths across the three functional zones further confirm substantial spatial heterogeneity in anthropogenic stressor drivers (Figures S3–S5). Soil erosion intensity was excluded from the eastern and central zone models due to convergence issues arising from zero variance and therefore does not appear in Figures S4(b) and S5(b). Overall, the zonal MGWR results are consistent with the regional findings, showing relatively stable coefficient distributions for most stressor and indicator nodes, while urbanization and those indicators related to urbanization exhibit greater variability in their estimated coefficients and bandwidths. Notably, the central urban development zone is characterized by uniformly small optimal bandwidths and tightly clustered indicator coefficients (Figure S5).

To further characterize the overall distribution and variability of driving effects across functional zones, regression coefficients of variables within the same driver category were pooled and treated as samples. Moreover, effect strength (local MGWR coefficients) and spatial scale (optimal bandwidths) were jointly synthesized for all BBN nodes, enabling a quadrant-based classification of node-specific influence patterns (Figure 13).



458 Figure 13. Local MGWR coefficient distributions and quadrant-based classification of BBN nodes. (a)
459 Distributions of local MGWR coefficients for anthropogenic stressor nodes; (b) Distributions of local
460 MGWR coefficients for plot-level indicator nodes; (c) Quadrant-based classification of BBN nodes
461 integrating spatial scale and effect strength. The vertical and horizontal red dashed lines represent the
462 median spatial scale (optimal bandwidth) and the median effect strength (absolute standardized
463 coefficient), respectively, dividing the plane into four quadrants: Q1 (lower right, global-scale–weak
464 effect), Q2 (lower left, local-scale–weak effect), Q3 (upper left, local-scale–strong effect), and Q4 (upper
465 right, global-scale–strong effect). The median spatial scale and effect strength are 170 km and 0.0037,

466 respectively. Abbreviations: AGRI, agricultural production; NON-CROP, non-cropping livelihood
467 activities; URBAN, urbanization; LIVESTOCK, livestock density; SLOPE, slope gradient; GDP, total
468 GDP; POP, population density; D2R, proximity to road; D2W, proximity to surface water; D2V, distance
469 to village; D2T, distance to township; D2C, distance to county.

470 Stressor coefficients exhibit pronounced zonal contrasts in both central tendency and
471 dispersion, with the central zone displaying the broadest and most diffuse distributions, as
472 evidenced by its wider violin shape, indicating strong variability in the magnitude of stressor
473 effects across locations (Figure 13(a)). In contrast, the northwest zone is characterized by
474 more tightly clustered coefficients, while the eastern zone shows intermediate levels of
475 dispersion. Turning to indicator coefficients, the central zone exhibits more symmetrically
476 distributed values concentrated around zero compared with the northwest and eastern zones,
477 suggesting comparatively stable and moderate indicator influences on risk (Figure 13(b)).
478 Across all zones, most plot-level indicators are predominantly associated with localized and
479 weak effects (Q2), whereas anthropogenic stressors generally exhibit stronger influences
480 operating at broader spatial scales (Q4), with urbanization emerging as a notable exception
481 characterized by localized but strong effects (Q3) (Figure 13(c)).

482 **4. Discussion**

483 These results provide several insights into the mechanisms underlying ecological risk
484 patterns captured by the proposed assessment framework.

485 **4.1 Dominant role of urbanization in cumulative anthropogenic stressor risk**

486 Anthropogenic stressors contribute unevenly to cumulative anthropogenic stressor risk, with
487 urbanization consistently emerging as the most sensitive driver, whose variations induce
488 larger fluctuations in cumulative risk than other stressors (Figure 9(a)). This heightened

sensitivity reflects the compound and systemic nature of urbanization, which simultaneously integrates land use conversion, population aggregation, infrastructure expansion, and intensified resource consumption, thereby amplifying its marginal influence on ecological risk (Elmqvist et al., 2019; Seto et al., 2012). Moreover, urbanization often operates near ecological thresholds and generates pronounced spatial spillover effects from urban cores into adjacent buffer zones, leading to nonlinear and spatially propagated risk responses (Groffman et al., 2006; Scheffer et al., 2001).

Accordingly, plot-level indicators closely associated with urbanization—particularly population density and distances to townships and counties—exhibit stronger direct and indirect effects on both urbanization and cumulative risk (Figure 9(b)). Potential urbanization areas are primarily concentrated in the southeastern plains (Figure 7(d)), where dense populations and clustered administrative centers generate more concentrated indicator patterns (Figures S1(i), S1(m), and S1(n)), reinforcing their determinative roles in predicting urbanization-related risk. In contrast, potential agricultural production and non-cropping livelihood activities are more widely distributed across the BTH region (Figures 7(b)–7(c)), resulting in more dispersed indicator patterns and comparatively weaker contributions to both specific and cumulative risks.

Collectively, these findings identify urbanization as a critical leverage point in shaping cumulative anthropogenic stressor risk, underscoring the necessity of explicitly accounting for compound stressors and incorporating additional plot-level socioeconomic indicators to improve the robustness and policy relevance of regional risk assessments.

4.2 Scale dependence of cumulative anthropogenic stressor risk and associated stressor

drivers

At the regional scale, variations in Spearman correlations across spatial resolutions reveal pronounced contrasts in the scale dependence of specific anthropogenic stressor risks. The steeper correlation declines observed for non-cropping livelihood activities and urbanization indicate stronger scale dependence (Figures 8(c)–8(d)), suggesting that these risks are shaped by fine-scale spatial heterogeneity that is progressively smoothed under spatial aggregation (Carroll et al., 2017; Wu, 2013). Given the dominant contribution of these two stressors to cumulative risk (86%), as derived from the CPTs (Figure 6), the cumulative risk exhibits a comparable pattern of scale-dependent variation (Figure 8(a)). In contrast, agricultural production risk shows strong cross-scale consistency in its spatial pattern (Figure 8(b)), suggesting that it is primarily governed by structurally persistent drivers—such as proximity to surface water and road—that remain coherent under spatial aggregation.

Spatial analyses further reveal pronounced spatial non-stationarity in key stressor drivers of cumulative risk, particularly non-cropping livelihood activities and urbanization. GWR results for these stressors exhibit wider interquartile ranges and elongated distribution tails, indicating substantial spatial heterogeneity in their local effects (Figure 11(a)). Consistent with Kang and Oshan (2025) and Feng et al. (2025), such heterogeneous coefficient patterns suggest that the relationships between these stressors and risk vary markedly across space and are sensitive to the scale at which they are assessed. In summary, these findings indicate that cumulative anthropogenic stressor risk and associated stressor drivers are inherently scale dependent, underscoring the importance of scale-aware and spatially differentiated

approaches in regional risk assessment and ecosystem management.

4.3 Scale-dependent risk effects shaped by socioeconomic processes across spatial levels

MGWR provides explicit insights into whether anthropogenic stressor risk drivers operate at distinct spatial scales. Variables closely associated with urbanization—namely total GDP, population density, and urbanization intensity—exhibit pronounced spatial heterogeneity in their local coefficients (Figures 12(a)–12(b)), indicating strong spatial variation in their risk effects. These patterns are further supported by the optimal MGWR bandwidths (Figure 12(c)). Most drivers are characterized by very large bandwidths (>600 km), suggesting spatially smooth or near-global effects, whereas urbanization- and distance-related drivers display substantially smaller bandwidths (≤212 km), reflecting more localized and spatially heterogeneous influences on cumulative anthropogenic stressor risk.

Zonal sensitivity patterns further contextualize these scale contrasts by revealing differences in response magnitude across functional zones. Relative to the BTH region as a whole, the eastern agricultural production zone exhibits markedly higher sensitivity to agricultural production– and non-cropping livelihood activity–related risks, while showing comparatively weaker responses to urbanization-related indicators (Figure 10). Consistent with the broader literature (Alberti, 2015; Lambin and Meyfroidt, 2011; Seto et al., 2012), this contrast reflects the dominance of agriculture-oriented socioeconomic processes that operate locally within production landscapes, whereas urbanization-related processes—despite their localized variability—shape regional risk patterns through spatial spillovers and cross-zone interactions. Taken together, these results indicate that scale-dependent risk

effects are heterogeneous and are jointly shaped by localized socioeconomic processes and their broader regional linkages.

4.4 Aligning risk mitigation strategies with scale-dependent drivers

Compared with the northwest ecological conservation and eastern agricultural production zones, the central urban development zone is characterized by smaller optimal MGWR bandwidths (Figure S5(c)) and relatively compact coefficient distributions within local neighborhoods for both stressor (Figure S5(a); Figure 13(a)) and indicator drivers (Figure S5(b); Figure 13(b)). Moreover, these drivers are predominantly concentrated in the Q2 and Q3 quadrants, indicating localized spatial scales with weak to strong effects (Figure 13(c)). Taken together, these patterns indicate that the central urban development zone is characterized by strong but locally structured variability, with stressor effects differing markedly in magnitude across space while remaining internally coherent within localized spatial domains.

This scale configuration implies that uniform, zone-wide planning instruments can effectively mitigate anthropogenic stressor risk without substantial loss of effectiveness due to spatial heterogeneity. Accordingly, risk mitigation strategies centered on land use regulation (He et al., 2025; Li et al., 2020) and the deployment of green infrastructure (Rahman et al., 2025; Seidu et al., 2025) are likely to be particularly effective in the central urban development zone, especially around major cities where urbanization stressor is most concentrated.

In contrast, the northwest ecological conservation and eastern agricultural production zones exhibit broader MGWR bandwidths and more dispersed coefficient distributions, indicating

that dominant risk drivers operate across larger spatial extents and display stronger spatial heterogeneity (Figures 13(a)–13(c); Figures S3–S4). These characteristics suggest that uniform, one-size-fits-all strategies are unlikely to be effective in these zones. Instead, risk mitigation strategies should be differentiated and explicitly scale-sensitive, with strategies tailored to dominant local processes. For example, fine-scale zoning schemes (Li et al., 2020), spatially differentiated buffer zones (Zheng et al., 2016), and livelihood diversification programs (Erbaugh and Oldekop, 2018) may be more effective in reducing production- and livelihood-related risks in these functionally heterogeneous landscapes.

5. Conclusion

Using the Beijing–Tianjin–Hebei region as a case study, this research proposes an integrated framework for assessing ecological risk from multiple anthropogenic stressors and their spatial variability. Cumulative risk, aggregated from agricultural production, non-cropping livelihood activities, and urbanization, exhibits pronounced spatial clustering, with urbanization emerging as a critical leverage point in shaping cumulative risk. These clustered high-risk areas delineate priority areas for conservation and targeted risk mitigation. The results highlight the importance of explicitly accounting for compound stressors and incorporating finer-scale socioeconomic indicators to enhance the robustness and policy relevance of ERAs. Ecological risk and its drivers are inherently scale-dependent. The effects of stressor drivers on risk are heterogeneous and are jointly shaped by localized socioeconomic processes and broader regional linkages. Consequently, uniform planning instruments are effective where stressor drivers display strong but locally structured spatial patterns, whereas differentiated, scale-sensitive mitigation strategies are required when

dominant drivers operate across broader and more heterogeneous spatial domains.

Declaration of Interest Statement

The authors declare no conflict of interest.

Acknowledgments

605 **References**

606 Alberti, M., 2015. Eco-evolutionary dynamics in an urbanizing planet. Trends in
607 Ecology & Evolution 30, 114-126. https://doi.org/10.1016/j.tree.2014.11.007.
608 Ayre, K.K., Landis, W.G., 2012. A Bayesian Approach to Landscape Ecological Risk
609 Assessment Applied to the Upper Grande Ronde Watershed, Oregon. Human and
610 Ecological Risk Assessment: An International Journal 18, 946-970.
611 https://doi.org/10.1080/10807039.2012.707925.
612 Bartell, S.M., 2008. Ecological Risk Assessment, in: Jørgensen, S.E., Fath, B.D. (Eds.),
613 Encyclopedia of Ecology. Academic Press, Oxford, pp. 1097-1101.
614 https://doi.org/10.1016/B978-008045405-4.00387-6.
615 Borsuk, M.E., Reichert, P., Peter, A., Schager, E., Burkhardt-Holm, P., 2006. Assessing
616 the decline of brown trout (Salmo trutta) in Swiss rivers using a Bayesian probability
617 network. Ecological Modelling 192, 224-244.
618 https://doi.org/10.1016/j.ecolmodel.2005.07.006.
619 Carriger, J.F., Barron, M.G., 2020. A Bayesian network approach to refining ecological
620 risk assessments: Mercury and the Florida panther (Puma concolor coryi). Ecological
621 Modelling 418, 108911. https://doi.org/10.1016/j.ecolmodel.2019.108911.
622 Carriger, J.F., Barron, M.G., Newman, M.C., 2016. Bayesian Networks Improve Causal
623 Environmental Assessments for Evidence-Based Policy. Environmental science &
624 technology 50, 13195-13205. https://doi.org/10.1021/acs.est.6b03220.
625 Carroll, C., Roberts, D.R., Michalak, J.L., Lawler, J.J., Nielsen, S.E., Stralberg, D.,
626 Hamann, A., McRae, B.H., Wang, T., 2017. Scale-dependent complementarity of

climatic velocity and environmental diversity for identifying priority areas for conservation under climate change. Global Change Biology 23, 4508-4520. https://doi.org/10.1111/gcb.13679.

CBD, 2022. Kunming-Montreal global biodiversity framework: CBD/COP/15/L.25, Montreal, Canada.

Chinese State Council, 2010. The main functional zone plan, Beijing.

Delignette-Muller, M.L., Dutang, C., 2015. fitdistrplus: An R Package for Fitting Distributions. Journal of Statistical Software 64, 1 - 34. https://doi.org/10.18637/jss.v064.i04.

Dormann, C.F., Calabrese, J.M., Guillera-Arroita, G., Matechou, E., Bahn, V., Bartoń, K., Beale, C.M., Ciuti, S., Elith, J., Gerstner, K., Guelat, J., Keil, P., Lahoz-Monfort, J.J., Pollock, L.J., Reineking, B., Roberts, D.R., Schröder, B., Thuiller, W., Warton, D.I., Wintle, B.A., Wood, S.N., Wüest, R.O., Hartig, F., 2018. Model averaging in ecology: a review of Bayesian, information-theoretic, and tactical approaches for predictive inference. Ecological Monographs 88, 485-504. https://doi.org/https://doi.org/10.1002/ecm.1309.

Dormann, C.F., Elith, J., Bacher, S., Buchmann, C., Carl, G., Carré, G., Marquéz, J.R.G., Gruber, B., Lafourcade, B., Leitão, P.J., Münkemüller, T., McClean, C., Osborne, P.E., Reineking, B., Schröder, B., Skidmore, A.K., Zurell, D., Lautenbach, S., 2012. Collinearity: a review of methods to deal with it and a simulation study evaluating their performance. Ecography 36, 27-46. https://doi.org/10.1111/j.1600-0587.2012.07348.x.

Du, W., Liao, X., Tong, Z., Rina, S., Rong, G., Zhang, J., Liu, X., Guo, E., 2023. Early

649 warning and scenario simulation of ecological security based on DPSIRM model and
650 Bayesian network: A case study of east Liaohe river in Jilin Province, China. Journal
651 of Cleaner Production 398, 136649. https://doi.org/10.1016/j.jclepro.2023.136649.
652 Eldridge, D.J., Delgado-Baquerizo, M., Travers, S.K., Val, J., Oliver, I., 2017. Do
653 grazing intensity and herbivore type affect soil health? Insights from a semi-arid
654 productivity gradient. Journal of Applied Ecology 54, 976-985.
655 https://doi.org/10.1111/1365-2664.12834.
656 Elmqvist, T., Andersson, E., Frantzeskaki, N., McPhearson, T., Olsson, P., Gaffney, O.,
657 Takeuchi, K., Folke, C., 2019. Sustainability and resilience for transformation in the
658 urban century. Nature Sustainability 2, 267-273. https://doi.org/10.1038/s41893-019-
659 0250-1.
660 Erbaugh, J.T., Oldekop, J.A., 2018. Forest landscape restoration for livelihoods and
661 well-being. Current Opinion in Environmental Sustainability 32, 76-83.
662 https://doi.org/10.1016/j.cosust.2018.05.007.
663 Feng, Y., Miao, Y., Turner, E., 2025. Examining spatial variations in the relationship
664 between domestic energy consumption and its driving factors using multiscale
665 geographically weighted regression: a case study in Nottingham, England. Energy,
666 Sustainability and Society 15, 24. https://doi.org/10.1186/s13705-025-00523-1.
667 Fenton, N., Neil, M., 2018. Risk Assessment and Decision Analysis with Bayesian
668 Networks (2nd edition). CRC Press, Boca Raton. https://doi.org/10.1201/b21982.
669 Fotheringham, A.S., 2008. Geographically weighted regression, in: Rogerson, P.A.,
670 Fotheringham, A.S. (Eds.), The SAGE handbook of spatial analysis. Sage Publications,

London, pp. 243-254.

Fotheringham, A.S., Yang, W., Kang, W., 2017. Multiscale Geographically Weighted Regression (MGWR). Annals of the American Association of Geographers 107, 1247-1265. https://doi.org/10.1080/24694452.2017.1352480.

Fu, B., Liu, Y., Meadows, M.E., 2023. Ecological restoration for sustainable development in China. National Science Review. https://doi.org/10.1093/nsr/nwad033.

Gao, X., Zhang, H., Huang, L., Fan, J., Liu, X., Cao, W., Liu, H., Liu, G., 2024. Where, When, and How Much Should We Pay for Wind Erosion Prevention Services of the Largest Chinese Grassland Reserve? Environmental science & technology 58, 2615-2626. https://doi.org/10.1021/acs.est.3c03327.

Gollini, I., Lu, B., Charlton, M., Brunsdon, C., Harris, P., 2015. GWmodel: An R Package for Exploring Spatial Heterogeneity Using Geographically Weighted Models. Journal of Statistical Software 63, 1 - 50. https://doi.org/10.18637/jss.v063.i17.

Gonzalez-Redin, J., Luque, S., Poggio, L., Smith, R., Gimona, A., 2016. Spatial Bayesian belief networks as a planning decision tool for mapping ecosystem services trade-offs on forested landscapes. Environmental research 144, 15-26. https://doi.org/10.1016/j.envres.2015.11.009.

Grantham, H.S., Duncan, A., Evans, T.D., Jones, K.R., Beyer, H.L., Schuster, R., Walston, J., Ray, J.C., Robinson, J.G., Callow, M., Clements, T., Costa, H.M., DeGemmis, A., Elsen, P.R., Ervin, J., Franco, P., Goldman, E., Goetz, S., Hansen, A., Hofsvang, E., Jantz, P., Jupiter, S., Kang, A., Langhammer, P., Laurance, W.F., Lieberman, S., Linkie, M., Malhi, Y., Maxwell, S., Mendez, M., Mittermeier, R.,

693 Murray, N.J., Possingham, H., Radachowsky, J., Saatchi, S., Samper, C., Silverman, J.,
694 Shapiro, A., Strassburg, B., Stevens, T., Stokes, E., Taylor, R., Tear, T., Tizard, R.,
695 Venter, O., Visconti, P., Wang, S., Watson, J.E.M., 2020. Anthropogenic modification
696 of forests means only 40% of remaining forests have high ecosystem integrity. Nature
697 communications 11, 5978. https://doi.org/10.1038/s41467-020-19493-3.
698 Groffman, P.M., Baron, J.S., Blett, T., Gold, A.J., Goodman, I., Gunderson, L.H.,
699 Levinson, B.M., Palmer, M.A., Paerl, H.W., Peterson, G.D., Poff, N.L., Rejeski, D.W.,
700 Reynolds, J.F., Turner, M.G., Weathers, K.C., Wiens, J., 2006. Ecological Thresholds:
701 The Key to Successful Environmental Management or an Important Concept with No
702 Practical Application? Ecosystems 9, 1-13. https://doi.org/10.1007/s10021-003-0142-z.
703 He, Y., Liu, X., Wu, D., Li, S., Zhou, P., 2025. Ecological Risks and Patterns Associated
704 With Land Use/Cover Changes Along the Belt and Road Initiative Routes. Land
705 Degradation & Development 36, 2075-2094. https://doi.org/10.1002/ldr.5483.
706 Helle, I., Jolma, A., Venesjärvi, R., Jones, J., 2016. Species and habitats in danger:
707 estimating the relative risk posed by oil spills in the northern Baltic Sea. Ecosphere 7.
708 https://doi.org/10.1002/ecs2.1344.
709 Huang, Y., Li, Z., 2025. Global mapping of freshwater contamination by pesticides and
710 implications for agriculture and water resource protection. iScience 28.
711 https://doi.org/10.1016/j.isci.2025.112861.
712 IPBES, 2019. Summary for policymakers of the global assessment report on
713 biodiversity and ecosystem services of the Intergovernmental Science-Policy Platform
714 on Biodiversity and Ecosystem Services. IPBES secretariat, Bonn, Germany.

715 Jarvis, A., Reuter, H.I., Nelson, A., Guevara, E., 2008, Hole-Filled SRTM for the Globe
716 Version 4, accessed on January 15, 2025.
717 Kaikkonen, L., Parviainen, T., Rahikainen, M., Uusitalo, L., Lehikoinen, A., 2021.
718 Bayesian Networks in Environmental Risk Assessment: A Review. Integr Environ
719 Assess Manag 17, 62-78. https://doi.org/10.1002/ieam.4332.
720 Kang, W., Oshan, T.M., 2025. Scale and correlation in multiscale geographically
721 weighted regression (MGWR). Journal of Geographical Systems 27, 399-424.
722 https://doi.org/10.1007/s10109-025-00468-1.
723 Kummu, M., Kosonen, M., Masoumzadeh Sayyar, S., 2025. Downscaled gridded global
724 dataset for gross domestic product (GDP) per capita PPP over 1990–2022. Scientific
725 data 12, 178. https://doi.org/10.1038/s41597-025-04487-x.
726 Lambin, E.F., Meyfroidt, P., 2011. Global land use change, economic globalization, and
727 the looming land scarcity. Proceedings of the National Academy of Sciences of the
728 United States of America 108, 3465-3472. https://doi.org/10.1073/pnas.1100480108.
729 Landuyt, D., Broekx, S., D'Hondt, R., Engelen, G., Aertsens, J., Goethals, P.L.M., 2013.
730 A review of Bayesian belief networks in ecosystem service modelling. Environmental
731 Modelling & Software 46, 1-11. https://doi.org/10.1016/j.envsoft.2013.03.011.
732 Landuyt, D., Van der Biest, K., Broekx, S., Staes, J., Meire, P., Goethals, P.L.M., 2015.
733 A GIS plug-in for Bayesian belief networks: Towards a transparent software framework
734 to assess and visualise uncertainties in ecosystem service mapping. Environmental
735 Modelling & Software 71, 30-38.
736 https://doi.org/https://doi.org/10.1016/j.envsoft.2015.05.002.

737 Li, H., Guan, Q., Sun, Y., Wang, Q., Liang, L., Ma, Y., Du, Q., 2022a. Spatiotemporal
738 analysis of the quantitative attribution of soil water erosion in the upper reaches of the
739 Yellow River Basin based on the RUSLE-TLSD model. CATENA 212, 106081.
740 https://doi.org/10.1016/j.catena.2022.106081.
741 Li, H., Ma, Z., Zhu, Y., Liu, Y., Yang, X., 2020. Planning and prioritizing forest
742 landscape restoration within megacities using the ordered weighted averaging operator.
743 Ecological Indicators 116, 106499. https://doi.org/10.1016/j.ecolind.2020.106499.
744 Li, H., Yang, X., Zhang, K., 2021. Understanding global land degradation processes
745 interacted with complex biophysics and socioeconomics from the perspective of the
746 Normalized Difference Vegetation Index (1982–2015). Global and Planetary Change
747 198, 103431. https://doi.org/10.1016/j.gloplacha.2021.103431.
748 Li, H., Zhang, X., Zhang, Y., Yang, X., Zhang, K., 2018. Risk assessment of forest
749 landscape degradation using Bayesian network modeling in the Miyun Reservoir
750 catchment (China) with emphasis on the Beijing–Tianjin sandstorm source control
751 program. Land Degradation & Development 29, 3876-3885.
752 https://doi.org/10.1002/ldr.3133.
753 Li, K., Yang, J., Wang, J., Wang, Z., Zeng, Y., Borrelli, P., Hubacek, K., Hu, Y., Xu, B.,
754 Fang, N., Zeng, C., Zhou, Z., Shi, Z., 2024. Human-altered soil loss dominates nearly
755 half of water erosion in China but surges in agriculture-intensive areas. One Earth 7,
756 2008-2018. https://doi.org/10.1016/j.oneear.2024.09.001.
757 Li, S., Yan, J., Pei, Q., Sha, J., Liu, F., 2022b. Dynamic Relationship Between Water
758 Resources and New Urbanization Based on a Vector Autoregressive Model: A Case

759 Study of Hebei Province, China. Front Env Sci-Switz 10.
760 https://doi.org/10.3389/fenvs.2022.941726.
761 Liu, J., Xu, X., Zou, C., Lin, N., Zhang, K., Shan, N., Zhang, H., Liu, R., 2023. A
762 Bayesian network-GIS probabilistic model for addressing human disturbance risk to
763 ecological conservation redline areas. Journal of environmental management 344,
764 118400. https://doi.org/10.1016/j.jenvman.2023.118400.
765 Liu, L., Cao, X., Li, S., Jie, N., 2024, GlobPOP: A 33-year (1990-2022) global gridded
766 population dataset generated by cluster analysis and statistical learning, accessed on
767 Sep 2nd, 2025. https://doi.org/10.5281/zenodo.7813301.
768 Liu, Y., Fang, F., Li, Y., 2014. Key issues of land use in China and implications for
769 policy making. Land Use Policy 40, 6-12.
770 https://doi.org/10.1016/j.landusepol.2013.03.013.
771 Lu, B., Yang, W., Ge, Y., Harris, P., 2018. Improvements to the calibration of a
772 geographically weighted regression with parameter-specific distance metrics and
773 bandwidths. Computers, Environment and Urban Systems 71, 41-57.
774 https://doi.org/10.1016/j.compenvurbsys.2018.03.012.
775 Magdoff, F., Van Es, H., 2021. Ch 6. Soil Degradation: Erosion, Compaction, and
776 Contamination, Building soils for better crops: Ecological management for healthy
777 soils. Sustainable Agriculture Research and Education, USA.
778 Malekmohammadi, B., Tayebzadeh Moghadam, N., 2018. Application of Bayesian
779 networks in a hierarchical structure for environmental risk assessment: a case study of
780 the Gabric Dam, Iran. Environmental monitoring and assessment 190, 279.

https://doi.org/10.1007/s10661-018-6609-3.

Marcot, B.G., 2006. Characterizing Species at Risk I: Modeling Rare Species Under the Northwest Forest Plan. Ecology & Society 11, 473-482.

Martinez-Megias, C., Mentzel, S., Fuentes-Edfuf, Y., Moe, S.J., Rico, A., 2023. Influence of climate change and pesticide use practices on the ecological risks of pesticides in a protected Mediterranean wetland: A Bayesian network approach. The Science of the total environment 878, 163018. https://doi.org/10.1016/j.scitotenv.2023.163018.

Meijer, J.R., Huijbregts, M.A.J., Schotten, K.C.G.J., Schipper, A.M., 2018. Global patterns of current and future road infrastructure. Environmental Research Letters 13, 064006. https://doi.org/10.1088/1748-9326/aabd42.

Meyer, H., Reudenbach, C., Wöllauer, S., Nauss, T., 2019. Importance of spatial predictor variable selection in machine learning applications – Moving from data reproduction to spatial prediction. Ecological Modelling 411, 108815. https://doi.org/10.1016/j.ecolmodel.2019.108815.

Ministry of Natural Resources, 2023. Notice on Issuing the "China Land Ecological Basic Zoning (trial)", in: Ministry of Natural Resources of the People's Republic of China (Ed.), Beijing.

National Bureau of Statistics, 2020, National statistical area and urban-rural classification codes, https://www.stats.gov.cn/sj/tjbz/tjyqhdmhcxhfdm/2020/index.html, accessed on Apr 28, 2024.

803 Nojavan A, F., Qian, S.S., Stow, C.A., 2017. Comparative analysis of discretization
804 methods in Bayesian networks. Environmental Modelling & Software 87, 64-71.
805 https://doi.org/10.1016/j.envsoft.2016.10.007.
806 Parente, L., Ehrmann, S., Hengl, T., Fritz, S., C., B., Malek, Ž., Fischer, C., Perez, K.,
807 Stanimirova, R., Meyer, C., Wisser, D., Cinardi, G., Sloat, L., 2025, Global Pasture
808 Watch - Annual livestock headcount maps for cattle, goats, sheep and horses at 1-km
809 2000–2022 (FAOSTAT-adjusted) (v1), accessed on Sep 1st, 2025.
810 https://doi.org/10.5281/zenodo.14933636.
811 Perez, S., German-Labaume, C., Mathiot, S., Goix, S., Chamaret, P., 2022. Using
812 Bayesian networks for environmental health risk assessment. Environmental research
813 204, 112059. https://doi.org/10.1016/j.envres.2021.112059.
814 Phan, T.D., Smart, J.C.R., Capon, S.J., Hadwen, W.L., Sahin, O., 2016. Applications of
815 Bayesian belief networks in water resource management: A systematic review.
816 Environmental Modelling & Software 85, 98-111.
817 https://doi.org/10.1016/j.envsoft.2016.08.006.
818 Pittarello, M., Ravetto Enri, S., Lonati, M., Lombardi, G., 2021. Slope and distance
819 from buildings are easy-to-retrieve proxies for estimating livestock site-use intensity in
820 alpine summer pastures. PLOS ONE 16, e0259120.
821 https://doi.org/10.1371/journal.pone.0259120.
822 Pollino, C.A., Woodberry, O., Nicholson, A., Korb, K., Hart, B.T., 2007.
823 Parameterisation and evaluation of a Bayesian network for use in an ecological risk
824 assessment. Environmental Modelling & Software 22, 1140-1152.

825 https://doi.org/10.1016/j.envsoft.2006.03.006.
826 Poole, D., Zhang, N.L., 2003. Exploiting contextual independence in probabilistic
827 inference. Journal of Artificial Intelligence Research 18, 263-313.
828 https://doi.org/10.1613/jair.1122.
829 Rahman, M.D.R., Kang, S., Lee, S., Lee, J., 2025. A green infrastructure planning
830 approach for enhanced flood control and resilience in urban areas. Land Use Policy 153,
831 107535. https://doi.org/10.1016/j.landusepol.2025.107535.
832 Raynor, E.J., Gersie, S.P., Stephenson, M.B., Clark, P.E., Spiegal, S.A., Boughton, R.K.,
833 Bailey, D.W., Cibils, A., Smith, B.W., Derner, J.D., Estell, R.E., Nielson, R.M.,
834 Augustine, D.J., 2021. Cattle Grazing Distribution Patterns Related to Topography
835 Across Diverse Rangeland Ecosystems of North America. Rangeland Ecology &
836 Management 75, 91-103. https://doi.org/10.1016/j.rama.2020.12.002.
837 Scheffer, M., Carpenter, S., Foley, J.A., Folke, C., Walker, B., 2001. Catastrophic shifts
838 in ecosystems. Nature 413, 591-596. https://doi.org/10.1038/35098000.
839 Seidu, S., Chan, D.W.M., Edwards, D.J., Owusu-Manu, D.-G., 2025. A systematic
840 review of green infrastructure and ecosystem-based technologies for climate resilience:
841 development trends, research outlook and future projections. Environmental Research
842 Letters 20, 083001. https://doi.org/10.1088/1748-9326/ade730.
843 Seto, K.C., Güneralp, B., Hutyra, L.R., 2012. Global forecasts of urban expansion to
844 2030 and direct impacts on biodiversity and carbon pools. Proceedings of the National
845 Academy of Sciences 109, 16083-16088. https://doi.org/10.1073/pnas.1211658109.
846 Shamdasani, Y., 2021. Rural road infrastructure & agricultural production: Evidence

847 from India. Journal of Development Economics 152, 102686.
848 https://doi.org/10.1016/j.jdeveco.2021.102686.
849 Sperotto, A., Molina, J.L., Torresan, S., Critto, A., Marcomini, A., 2017. Reviewing
850 Bayesian Networks potentials for climate change impacts assessment and management:
851 A multi-risk perspective. Journal of environmental management 202, 320-331.
852 https://doi.org/10.1016/j.jenvman.2017.07.044.
853 Suter, G.W., Norton, S.B., 2019. Ecological Risk Assessment☆, in: Fath, B. (Ed.),
854 Encyclopedia of Ecology (Second Edition). Elsevier, Oxford, pp. 402-406.
855 https://doi.org/10.1016/B978-0-12-409548-9.11137-6.
856 Turner, W.R., Brandon, K., Brooks, T.M., Gascon, C., Gibbs, H.K., Lawrence, K.S.,
857 Mittermeier, R.A., Selig, E.R., 2012. Global Biodiversity Conservation and the
858 Alleviation of Poverty. BioScience 62, 85-92. https://doi.org/10.1525/bio.2012.62.1.13.
859 United Nations, 2024. The Global Threat of Drying Lands. United Nations.
860 https://doi.org/10.18356/9789295128163.
861 Urban, M.C., 2024. Climate change extinctions. Science 386, 1123-1128.
862 https://doi.org/doi:10.1126/science.adp4461.
863 USEPA, 2025. Ecological Risk Assessment.
864 Uusitalo, L., 2007. Advantages and challenges of Bayesian networks in environmental
865 modelling. Ecological Modelling 203, 312-318.
866 https://doi.org/10.1016/j.ecolmodel.2006.11.033.
867 Wang, X., Xiao, X., Qin, Y., Dong, J., Wu, J., Li, B., 2022. Improved maps of surface
868 water bodies, large dams, reservoirs, and lakes in China. Earth Syst. Sci. Data 14, 3757-

3771. https://doi.org/10.5194/essd-14-3757-2022.

Wang, Y., Lü, Y., Lü, D., Wu, X., Zhang, J., Li, T., Wang, X., 2024. Progress and gaps in ecological risk under climate change research: A bibliometric and literature review approach. Transactions in Earth, Environment, and Sustainability 2, 161-190. https://doi.org/10.1177/2754124x251323691.

Wu, J., 2013. Landscape sustainability science: ecosystem services and human well-being in changing landscapes. Landscape Ecology 28, 999-1023. https://doi.org/10.1007/s10980-013-9894-9.

Yang, J., Huang, X., 2024, The 30 m annual land cover datasets and its dynamics in China from 1985 to 2022, accessed on November 20, 2024. https://doi.org/10.5281/zenodo.4417809.

Zhang, W., 2021, Dataset of Soil Erosion Intensity with 300 m resoluton in 20 countries in key regions (2015), https://data.tpdc.ac.cn/en/data/44bbcc76-fdce-4197-9d7b-dc3528537f97/, accessed on January 12, 2025. https://doi.org/10.11888/Soil.tpdc.271737.

Zheng, H., Li, Y., Robinson, B.E., Liu, G., Ma, D., Wang, F., Lu, F., Ouyang, Z., Daily, G.C., 2016. Using ecosystem service trade-offs to inform water conservation policies and management practices. Frontiers in Ecology and the Environment 14, 527-532. https://doi.org/10.1002/fee.1432.

Zhou, W., Huang, G., Cadenasso, M.L., 2011. Does spatial configuration matter? Understanding the effects of land cover pattern on land surface temperature in urban landscapes. Landscape and Urban Planning 102, 54-63.

https://doi.org/10.1016/j.landurbplan.2011.03.009.